**AFRL-SN-RS-TR-2005-388**
**Final Technical Report**
**December 2005**

# SYNTHETIC APERTURE RADAR-MOVING TARGET INDICATION (SAR-MTI) PROCESSING OF MULTI-CHANNEL AIRBORNE RADAR MEASUREMENT (MCARM) DATA

**State University of New York at Buffalo**

*APPROVED FOR PUBLIC RELEASE; DISTRIBUTION UNLIMITED.*

**AIR FORCE RESEARCH LABORATORY**
**SENSORS DIRECTORATE**
**ROME RESEARCH SITE**
**ROME, NEW YORK**

**STINFO FINAL REPORT**

This report has been reviewed by the Air Force Research Laboratory, Information Directorate, Public Affairs Office (IFOIPA) and is releasable to the National Technical Information Service (NTIS). At NTIS it will be releasable to the general public, including foreign nations.

AFRL-SN-RS-TR-2005-388 has been reviewed and is approved for publication

APPROVED:     /s/

        BRAHAM HIMED
        Project Engineer

FOR THE DIRECTOR:     /s/

        RICHARD G. SHAUGHNESSY, Chief
        Rome Operations Office
        Sensors Directorate

# REPORT DOCUMENTATION PAGE

*Form Approved*
*OMB No. 074-0188*

| 1. AGENCY USE ONLY (Leave blank) | 2. REPORT DATE<br>DECEMBER 2005 | 3. REPORT TYPE AND DATES COVERED<br>Final   Oct 01 – Aug 04 |
|---|---|---|

**4. TITLE AND SUBTITLE**
SYNTHETIC APERTURE RADAR-MOVING TARGET INDICATION (SAR-MTI) PROCESSING OF MULTI-CHANNEL AIRBORNE RADAR MEASUREMENT (MCARM) DATA

**5. FUNDING NUMBERS**
C    - F30602-01-1-0544
PE   - 62204F
PR   - 762R
TA   - SN
WU  - P7

**6. AUTHOR(S)**
Braham Himed and
Mehrdad Soumekh

**7. PERFORMING ORGANIZATION NAME(S) AND ADDRESS(ES)**
State University of New York at Buffalo
The UB Commons
520 Lee Entrance
Suite 211
Amherst New York 14228

**8. PERFORMING ORGANIZATION REPORT NUMBER**

N/A

**9.  SPONSORING / MONITORING AGENCY NAME(S) AND ADDRESS(ES)**
Air Force Research Laboratory/SNRT
26 Electronic Parkway
Rome New York 13441-4514

**10. SPONSORING / MONITORING AGENCY REPORT NUMBER**

AFRL-SN-RS-TR-2005-388

**11. SUPPLEMENTARY NOTES**

AFRL Project Engineer:  Braham Himed/SNRT/(315) 330-2551/ Braham.Himed@rl.af.mil

**12a. DISTRIBUTION / AVAILABILITY STATEMENT**
APPROVED FOR PUBLIC RELEASE; DISTRIBUTION UNLIMITED.

**12b. DISTRIBUTION CODE**

**13. ABSTRACT** *(Maximum 200 Words)*
This report examines coherent signal processing methods for combining the data that are collected via a multi-channel airborne radar system for moving target detection and image formation.  We study methods that convert multi-channel radar data into dual along-track monopulse Synthetic Aperture Radar (SAR) signals of the radiated scene.  A two dimensional (2D) adaptive filtering method, that projects the data in one synthesized SAR channel into the signal subspace of the other, is used for blind calibration of the monopulse SAR signals and generation of the Moving Target Indication (MTI) statistic.  The merits of these algorithms are studied using the data from the Multi-Channel Airborne Radar Measurement (MCARM) system that has been developed by the Air Force Research Laboratory at Rome, New York.

**14. SUBJECT TERMS**
MCARM Data, Along Track Interferometry, Radar Signal Processing, Subspace Processing, Global Calibration, Local Calibration, Synthetic Aperture Radar, SAR, Moving Target Detection, GMTI

**15. NUMBER OF PAGES**
46

**16. PRICE CODE**

| 17. SECURITY CLASSIFICATION OF REPORT | 18. SECURITY CLASSIFICATION OF THIS PAGE | 19. SECURITY CLASSIFICATION OF ABSTRACT | 20. LIMITATION OF ABSTRACT |
|---|---|---|---|
| UNCLASSIFIED | UNCLASSIFIED | UNCLASSIFIED | UL |

# Table of Contents

# List of Figures

# 1. INTRODUCTION

The Department of Defense has been developing prototype multi-channel airborne radar systems to improve its capability for intelligence gathering, surveillance and reconnaissance. These airborne array radar systems are intended to collect rich databases that could be exploited for various tasks such as moving target detection and tracking, target imaging and recognition, etc. The multi-channel airborne radar systems provide a large volume of multi-dimensional information regarding the imaging scene that is being interrogated. For these systems, the task of a radar signal processor is to develop information processing algorithms that fully exploit the measured large-volume multi-channel airborne radar databases. Some of the issues include interpreting and/or coherently combining the airborne array data via imaging algorithms of Synthetic Aperture Radar (SAR), calibrating the data in various channels to detect subtle information that are critical for Airborne/Ground Moving Target Indicator (A/GMTI) problems, etc.

The Multi-Channel Airborne Radar Measurement (MCARM) [1] program was developed at the Air Force Research Laboratory (AFRL), in Rome, New York. Under this program, multi-channel clutter data were collected using an L-band active aperture and multiple IF receivers. A British Aerospace Corporation (BAC) 1-11 was used as a platform for the L-band ($f_0 = 1.25$GHz) radar data collection system. A 20kW peak transmit power was used for all data collections. The MCARM database is comprised of pre-processed airborne radar datacubes. Each acquisition data file consists of a single coherent processing interval (CPI). The data was collected at a variety of pulse repetition frequencies (PRFs) and over various terrains including mountains, rural, urban, and littoral regions. Monostatic data was collected at PRFs of 27 kHz (High PRF), 2 kHz (Medium PRF), and 500 Hz (Low PRF). The MCARM data was collected during several Delmarva and East Coast fly-overs terminating in Florida. During the MCARM flight test, data was collected simultaneously from a multi-channel sub-aperture architecture and a low sidelobe sum ($\Sigma$) and delta ($\Delta$) analog beamformer. The multi-channel architecture was tested using two separate sub-aperture configurations each having 22 degrees of freedom (DOF) (receivers). The receive antenna has 32 half-column arrays; each with 4 receiving antenna elements. For the Flight 5 case analyzed in this report, the MCARM antenna manifold consisted of two sets of eleven half-column arrays of four elements as shown in Figure 1. The planar array is composed of 22 half-column arrays each with four radiating elements spaced by 5.54 inches. The spacing between adjacent columns is 4.3 inches. The array is tilted 5° down from the vertical and is positioned approximately 2 feet from the fuselage surface. A linear frequency modulated (LFM) signal of 0.8 µsec (compressed pulse) with a compression of 63 was used. The receiver bandwidth is 0.8MHz. A set of measured steering vectors, each consisting of 129 points was also included. Test signals were also injected as part of the calibration process. To date, there are over 500 acquisitions for download for interested researchers.

The MCARM data were primarily collected for the exploration of adaptive array processing algorithms such as Space Time Adaptive Processing (STAP). Results on using STAP for the MCARM data are available in the literature [2-9]. The primary focus of our work is to interpret and process the MCARM data via SAR-based imaging and MTI algorithms; this will aid us to develop efficient means of pre-screening multi-channel radar data for potential moving target signals, and select subsets of data to subject to more computationally-intensive analysis. Such SAR-based signal processing algorithms have not yet been attempted with the MCARM

data, since this airborne radar system possesses a relatively small bandwidth (0.8 MHz) and synthetic aperture (less than 8 m at its medium PRF of 2 KHz).  These result in a relatively poor range-dependent resolution, e.g., 150 by 150 m at the range of 8 km.  Note, however, that certain conventional SAR systems possess even worse resolution.  Moreover, the signal measured via an individual receiver (with an aperture of a few centimeters) did not have sufficient power to yield an image with a good fidelity.

The first challenge we faced in developing a SAR-based imaging algorithm for the MCARM data was the small synthetic aperture size (8 m) relative to the azimuth extent of the illuminated target area (more than 80 km for the wide-beamwidth MCARM).  For such a scenario, the approximation-based polar format processing is not suitable.  Both the Fresnel approximation-based (also called range-Doppler algorithm [17]) and error-free wavefront SAR imaging algorithms would work for the MCARM database.  However, both methods require processing an extensively zero-padded aperture.  In this report, we present a simple and computationally inexpensive method to form spatial (slant-range and azimuth) images from the MCARM data.  This is achieved via a coherent processing of all 22 receive channels.  This processing is based on a global calibration and summation of these channels.

As mentioned earlier, the MCARM data were studied using STAP for MTI purposes [2-9].  It has been shown that STAP is a powerful and sophisticated tool for analyzing airborne array radar data.  However, STAP algorithms utilize complex matrix operations, often in an iterative fashion, to derive its final solution.  Several problems arise when operating STAP on measured data.  Assume for example that our radar system consists of an array of J spatial channels, collecting N pulses over L unambiguous range cells. The resulting covariance matrix has dimension JN by JN.  Computational complexity and the non-homogeneous nature of the airborne radar environment represent two reasons for developing reduced-dimension and reduced-rank techniques.  These methods involve linear transformations, such as from the time-domain to the frequency-domain or from the space-time domain to an orthonormal eigen-based coordinate system, and then a selection procedure is used to reduce the adaptive processor's degrees of freedom.

It has been shown that these alternative STAP methods often effectively cancel the interference of the transformed signal at significant computational savings.  In addition, less stringent secondary data requirements make the reduced-dimension/reduced-rank techniques more pragmatic in commonly encountered operational scenarios.  The question one might pose is whether there are simpler MTI processing methods that can be used to pre-screen the MCARM data, and identify segments of the data where a moving target may exist with a high probability of detection.  A more sophisticated algorithm such as STAP can then analyze the selected segments that incorporate a smaller database.

We use a SAR-based MTI method to achieve this pre-screening of the MCARM data. The proposed approach is based on an along-track monopulse SAR system. The along track monopulse SAR imaging system utilizes two radars for its data collection.  One radar is used as a transmitter as well as a monostatic receiver. The other radar is used only as a bistatic receiver. We have developed a signal processing algorithm of the two monostatic and bistatic databases of the along track monopulse SAR system to obtain two coherently identical SAR images of the stationary targets in the scene [10], [12 Sec. 8.1]. While the stationary targets appear the same in the monostatic and bistatic SAR images, however, the same is not true for moving targets. Thus,

the difference of the processed monostatic and bistatic data yields a statistic that is suitable for MTI.

This operation is feasible only if the two radars are fully calibrated; i.e., there is no relative gain and phase ambiguity in the data collected by the two radars. This idealistic scenario, however, is never encountered in practice. In a realistic monopulse SAR system, the two radars exhibit different patterns (phase as well as gain). These patterns vary with the radar operating frequency and the radar position (i.e., the slow-time) [12, Sec. 8.2]. Moreover, these patterns vary from one pulse transmission to another due to heat and other uncontrollable natural factors, which affect the internal circuitry of the two radars. These subtle changes of the radar patterns are difficult to detect and track, and are unknown to the user.

We have developed a practical multi-dimensional adaptive filtering method, called Signal Subspace Processing (SSP), to blindly calibrate the two channels of an along-track monopulse SAR system [11], [12, Sec. 8.3]. The SSP algorithm is applied in the SAR image domain within a small moving window to account for the spatially varying nature of the calibration errors of the two radars. This has been successfully applied to a dual channel along-track monopulse X-band SAR system [13].

We provide a study on the manner the 22 channels of MCARM system are interpreted for processing via the above-mentioned along-track monopulse SAR-MTI algorithm, and spatially-varying blind calibration of the resultant synthesized channels via the SSP algorithm. Three schemes for this purpose are examined. These methods attempt to improve MTI statistic by increasing SNR via average elements, expanding along track baseline, and/or speckle averaging. The results of processing the MCARM data via these three methods are provided.

## 2. MCARM SAR-MTI PROCESSING

### 2.1. MCARM System

The MCARM system used in this study is shown in Figure 1. In the transmit mode, all sub-apertures of the system are used in a phased array configuration to irradiate the target scene. The data were collected using a wide beamwidth and narrow beamwidth radiation patterns (via appropriate phasing of the transmitting sub-apertures). We studied acquisitions re050145 - re050155 from flight 5 and cycle e, which possess a wide beamwidth. Our results for these cases will show that the radar possessed a mainlobe beamwidth angle of over 150°. The imaging scene was a bay area (land and water) and a Moving Target Simulator (MTS). Examples of these will be studied in Section IV (Figures 5-7).
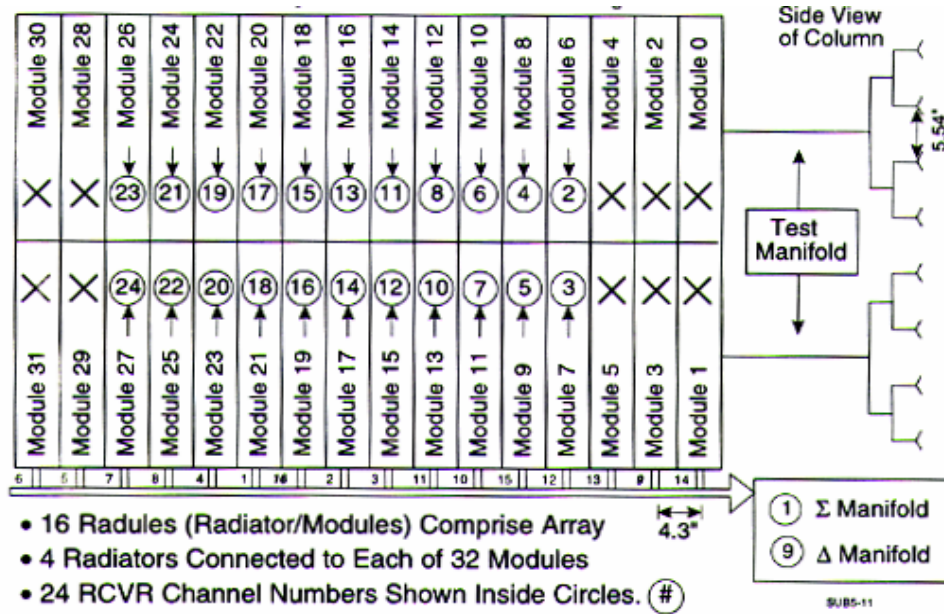


**Figure 1: MCARM System**

We also examined the databases with a narrow beamwidth. These include acquisitions from flight 5 and cycle d, rd050560, rd050614, and rd050644 for which the beam was directed at the transmit/receive azimuth (Xmit/Rece Az) Point Index of 55; rd050520, rd050575, and rd050628 for which the beam was directed at the Xmit/Rece Az Point Index of 65; and rd050480 for which the beam was directed at the Xmit/Rece Az Point Index of 75. All the narrow beamwidth exhibited a mainlobe beamwidth angle of 30° with significant sidelobes. The imaging scene was a land area west of Atlantic City, New Jersey. We will also provide examples of these databases in Section IV (Figures 8-11).

In the receive-mode, 22 sub-apertures were used to record the echoed signals. In Figure 1, these are identified as Modules 2-8 and 10-24. For simplicity, we refer to these as Receiver Elements 1-22. Our study (calibration results) indicates that the transmit-mode phase (time) delays were not turned off during the individual receptions of the 22 elements. For instance, the databases rd050560, rd050614 and rd050644, for which the beam was directed at the Xmit/Rece Az Point Index of 55, possessed similar calibration data.

## 2.2. SAR Representation of MCARM Data

As we stated in Section II.A, in the transmit-mode the MCARM system used all of its sub-apertures (12 elements in each of its two rows in range) in a phased array configuration to radiate the target scene; in the receive-mode, 22 sub-apertures (elements) were used to record the echoed signals. This corresponds to a *multi-static* radar data acquisition. However, due to the fact that the transmitting and receiving elements are within a small physical area, the resultant multi-static data may be viewed as monostatic SAR data as the coordinates of the platform are varied [18]. For instance, for the n-th receiving element, the continuous domain measured signal can be identified as $s_n(t,u)$, where $t$ represents the fast-time domain (in seconds) and $u$ denotes the synthetic aperture or the slow-time domain (in meters).

Such a SAR signal can be used to image the target scene. For the MCARM scenario where the target area is relatively large in the azimuth domain while the synthetic aperture is small (128 Pulse Repetition Intervals), polar format processing or Fresnel approximation-based imaging would fail. One can use the error-free SAR wavefront reconstruction algorithm [12]. However, that would require an extremely large amount of zero padding in the aperture domain to avoid circular convolution aliasing.

An approximation-based yet practical alternative is to use the far field model that is used in array processing literature (angle of arrival). For this, let the (Doppler) Fourier transform of the received signal with respect to the slow-time be

$$S_n(t,k_u) = \Im_{(u)}[s_n(t,u)], \tag{1}$$

where $k_u$ represents the synthetic aperture frequency domain or, as in the classical SAR literature, the Doppler domain.

Then, the target reconstruction is achieved via the following mapping:

$$f(x,y) = S_n(t,k_u), \tag{2}$$

where

$$x = r\cos\theta \qquad \text{and} \qquad y = r\sin\theta \tag{3}$$

and

$$r = \frac{ct}{2} \qquad \text{and} \qquad \theta = \arcsin\left(\frac{k_u}{2k_c}\right); \tag{4}$$

$(r,\theta)$ are the polar coordinates for the imaging scene in the spatial domain. In the above, $c$ is the wave propagation speed, and $k_c$ is the wavenumber at the carrier radar frequency. Note that the angular coordinate of a reflector $\theta$ is related to the Doppler frequency $k_u$ (as in the far-field approximations that are used in the classical array processing for *angle of arrival estimation* using small apertures).

Note that in theory; the above target function can be formed using the received signal of any of the 22 elements. However, in practice due to noise and other sources of errors, a one-element imaging does not yield a high fidelity image. Thus, our first task is to combine/add the

data of the 22 elements. However, there is a practical impasse in doing so. This is described and treated next.

## 2.3. Global Calibration of MCARM Data

Let the signal $s_1(t,u)$, recorded by the first element, be the reference signal. For a stationary scene and when the elements possess a common radiation pattern, the signal that is recorded by the n-th element is related to the reference signal via

$$s_n(t,u) = a_n \, s_1(t,u+u_n). \tag{5}$$

where $a_n$ is a complex number that represents a difference in gain and phase of the two signals. One source of this gain/phase is the relative physical distance of the n-th element from the first element in the slant-range domain. $u_n$ is the relative shift of the data in the slow-time domain; this shift is primarily due to the relative physical distance of the n-th element to the first element in the along-track (azimuth) domain. Both $(a_n, u_n)$ are also dependent of the internal circuitry of the two elements.

The above is a relatively simplistic way to relate the recorded signals, which assumes that the signals that are recorded by the two elements are related by a global gain/phase and slow-time delay (both of which are unknown). We will treat this problem via a more complicated model later. However, to get started, we solve for these global parameters $(a_n, u_n)$ via constructing the two-dimensional (2D) cross-correlation of $s_n(t,u)$ and the reference signal $s_1(t,u)$. Using this 2D correlation function, we can obtain an estimate of the relative gain and phase (i.e., $a_n$), and the sub-pixel slow-time shift (i.e., $u_n$; our study did not indicate any significant shift in the fast-time domain). (For sub-pixel accuracy, the 2D spectrum of each signal is zero-padded by a factor of 4 prior to constructing the cross-correlation function.)

Let $(\hat{a}_n, \hat{u}_n)$ be the estimates for the global calibration of the n-th signal with respect to the reference signal. Then, the signals from all elements could be coherently combined via

$$\hat{s}(t,u) = \sum_{n=1}^{22} \frac{1}{\hat{a}_n} s_n(t,u-\hat{u}_n). \tag{6}$$

Note that $(\hat{a}_1, \hat{u}_1) = (1,0)$. The SAR images that are formed in our study are generated using the cumulative 22-channel SAR signal $\hat{s}(t,u)$.

Figures 2a-d show estimates of the slow-time delay $\hat{u}_n$ for some of the wide-beamwidth and narrow-beamwidth MCARM databases; the estimates are separately shown versus the upper and lower MCARM elements. In the case of calibrated and evenly-spaced elements, the estimated slow-time delays should exhibit a linear behavior versus the upper elements 1, 3, 5… (Modules 6, 8, …, 26) in Figure 1; the same linear behavior should be present for the lower elements 2, 4, 6 … (Modules 7, 9, …, 27 in Figure 1).
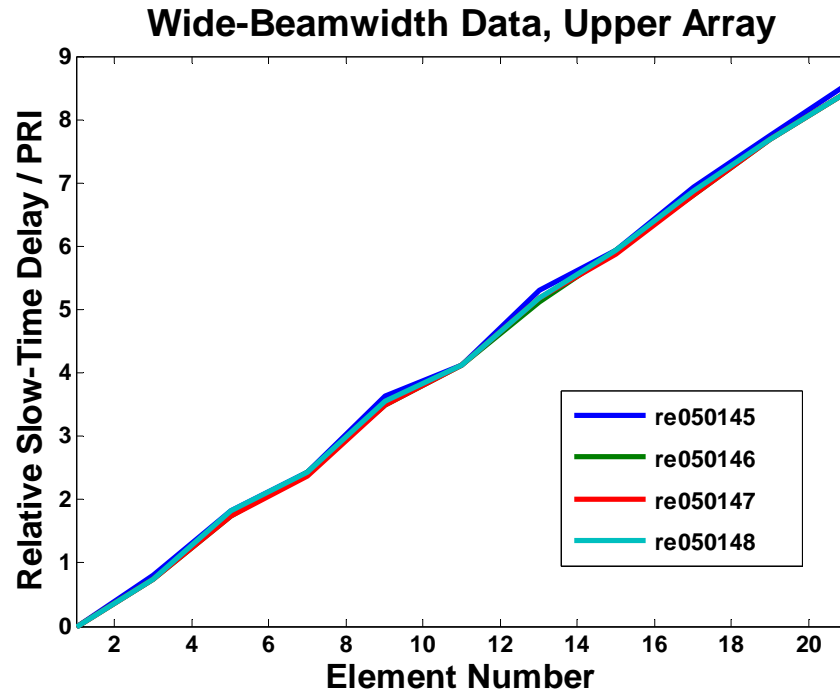
6

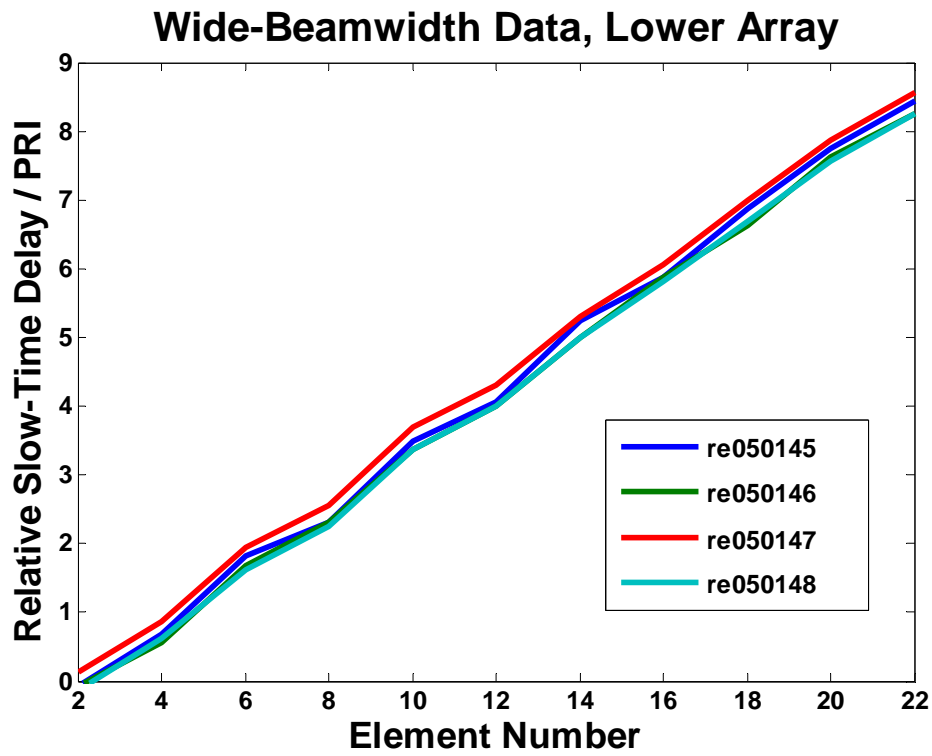**Figure 2a: Estimated slow-time delay, Wide-beamwidth Data, Upper Array**



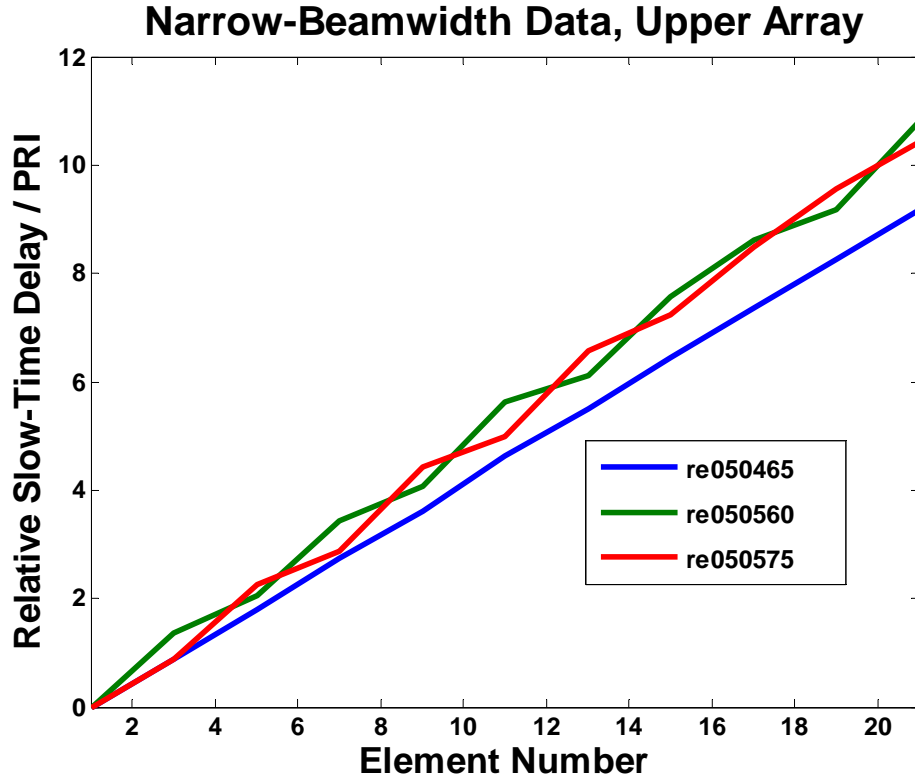**Figure 2b: Estimated slow-time delay, Wide-beamwidth Data, Lower Array**

**Figure 2c:  Estimated slow-time delay, Narrow-beamwidth Data, Upper Array**



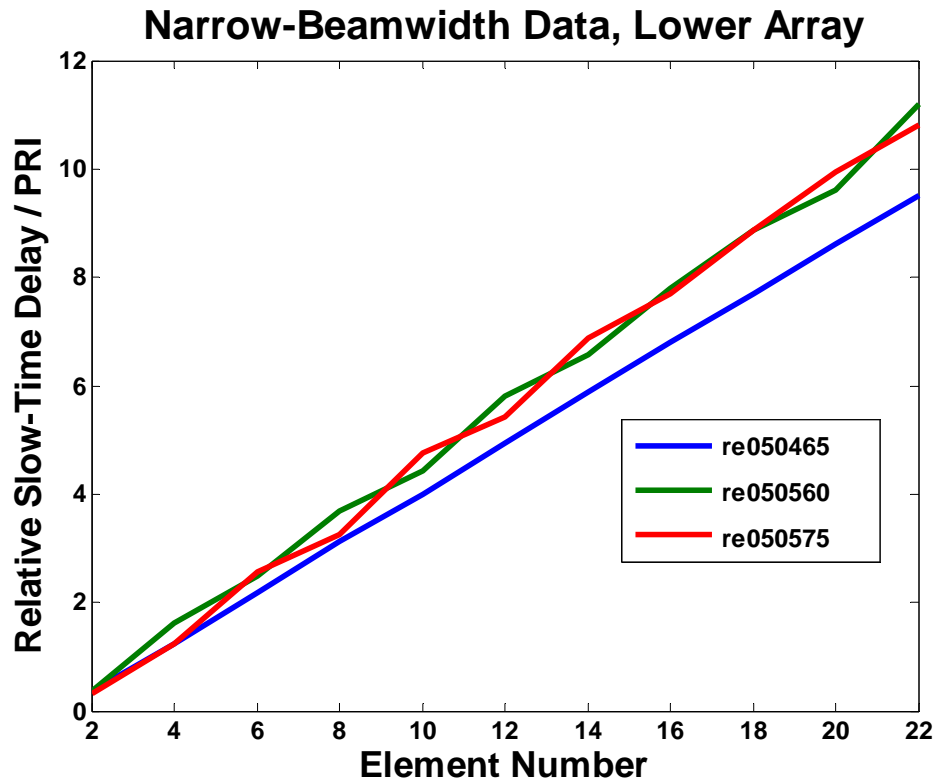**Figure 2d:  Estimated slow-time delay, Narrow-beamwidth Data, Lower Array**

Figures 2a-d indicate non-linear and unpredictable behaviors in the slow-time delay estimates though the MCARM elements were designed to be evenly-spaced in the spatial domain. Moreover, the estimates show variations from one database to another.
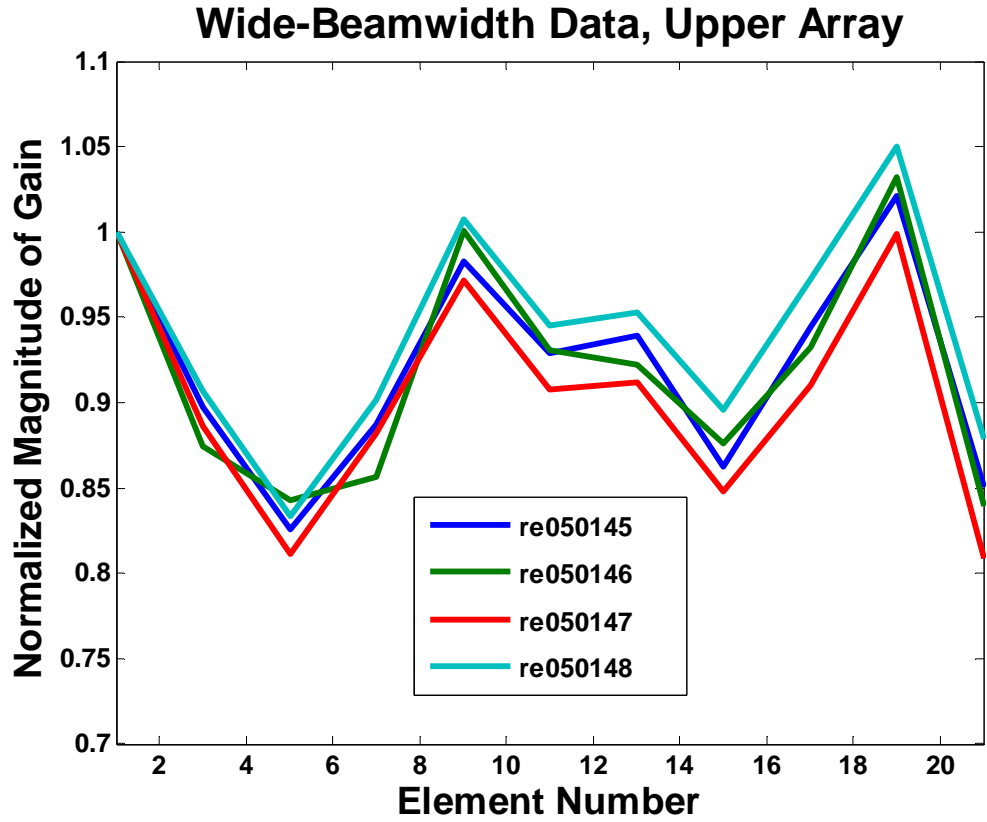


**Figure 3a:  Estimated magnitude of complex gain, Wide-beamwidth Data, Upper Array**

**Figure 3b: Estimated magnitude of complex gain, Wide-beamwidth Data, Lower Array**



**Figure 3c: Estimated phase of complex gain, Wide-beamwidth Data, Upper Array**

**Figure 3d: Estimated phase of complex gain, Wide-beamwidth Data, Lower Array**

The estimates of the complex weights $\hat{a}_n$ (magnitude and phase) also exhibit unpredictable non-linear behavior; these are shown in Figures 3a-d for the wide-beamwidth data, and Figures 3e-h for the narrow-beamwidth data.

**Narrow-Beamwidth Data, Upper Array**



**Figure 3e: Estimated magnitude of complex gain, Narrow -beamwidth Data, Upper Array**

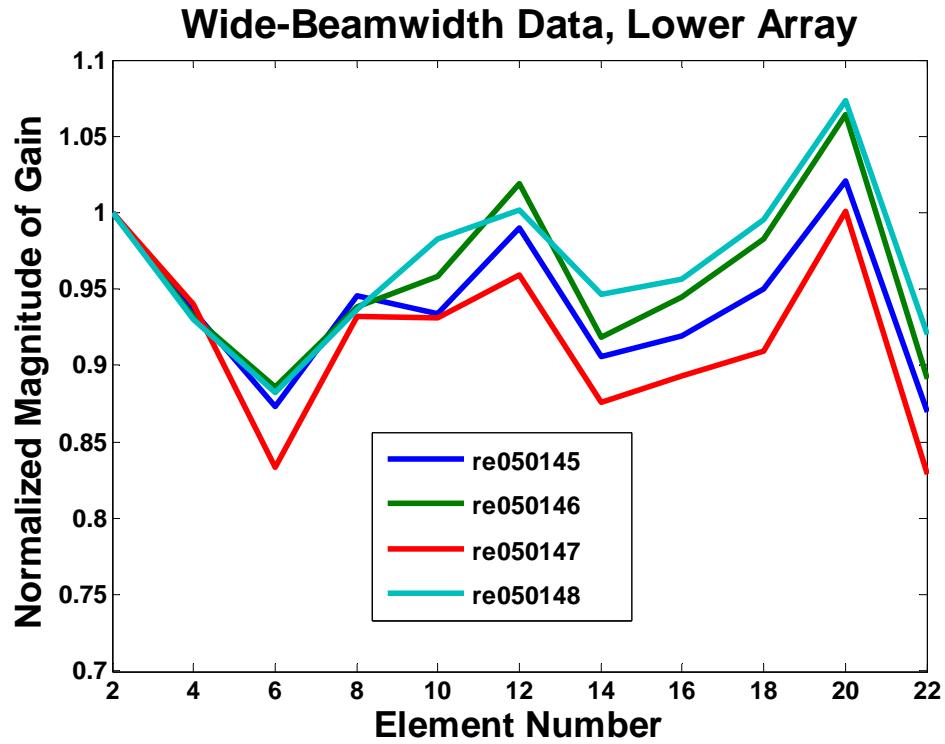**Narrow-Beamwidth Data, Lower Array**



**Figure 3f: Estimated magnitude of complex gain, Narrow -beamwidth Data, Lower Array**
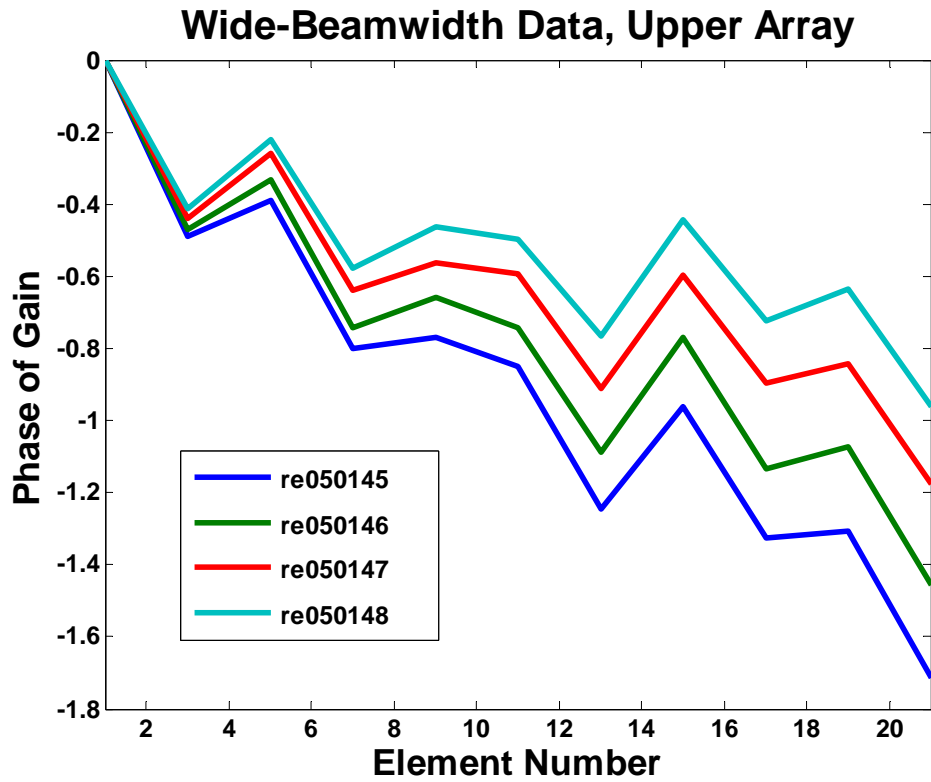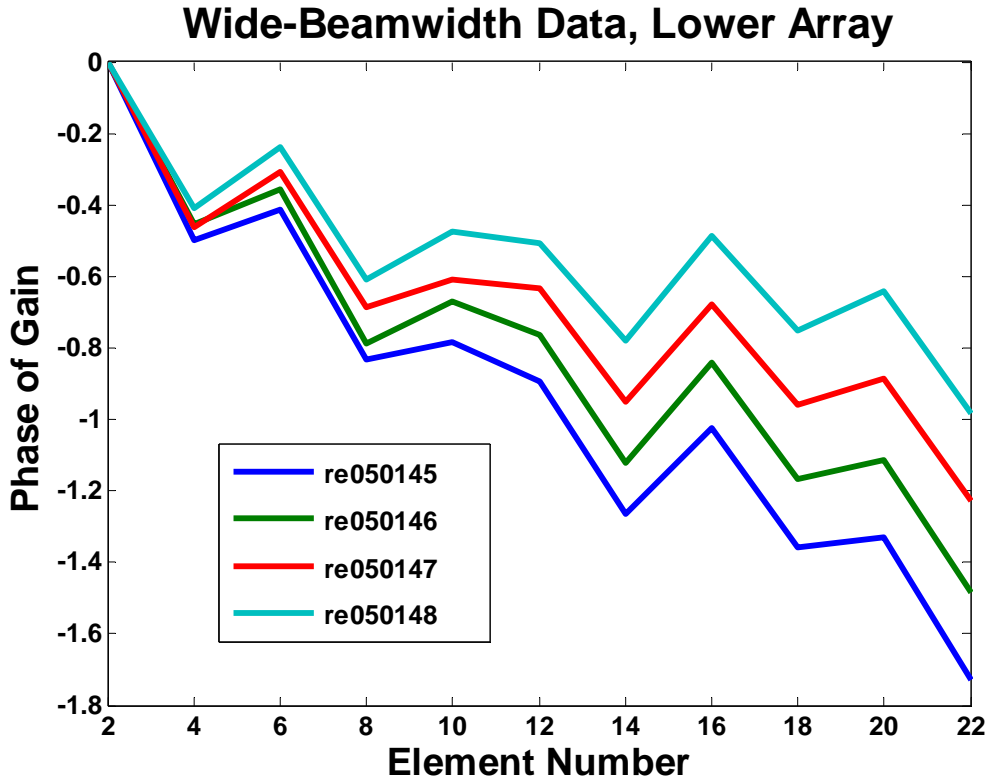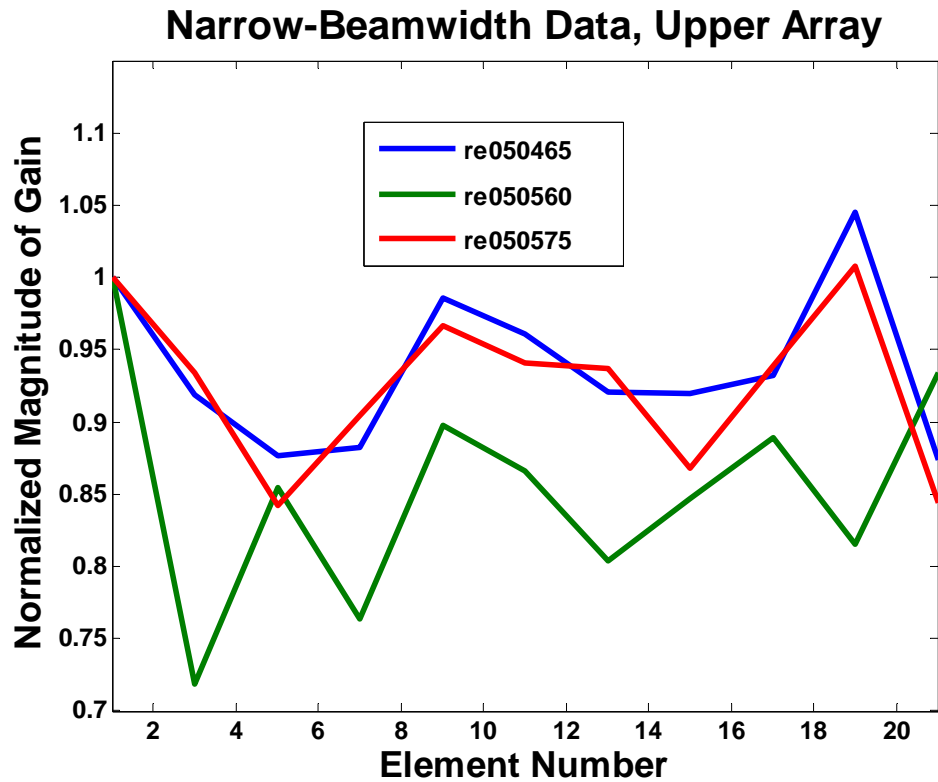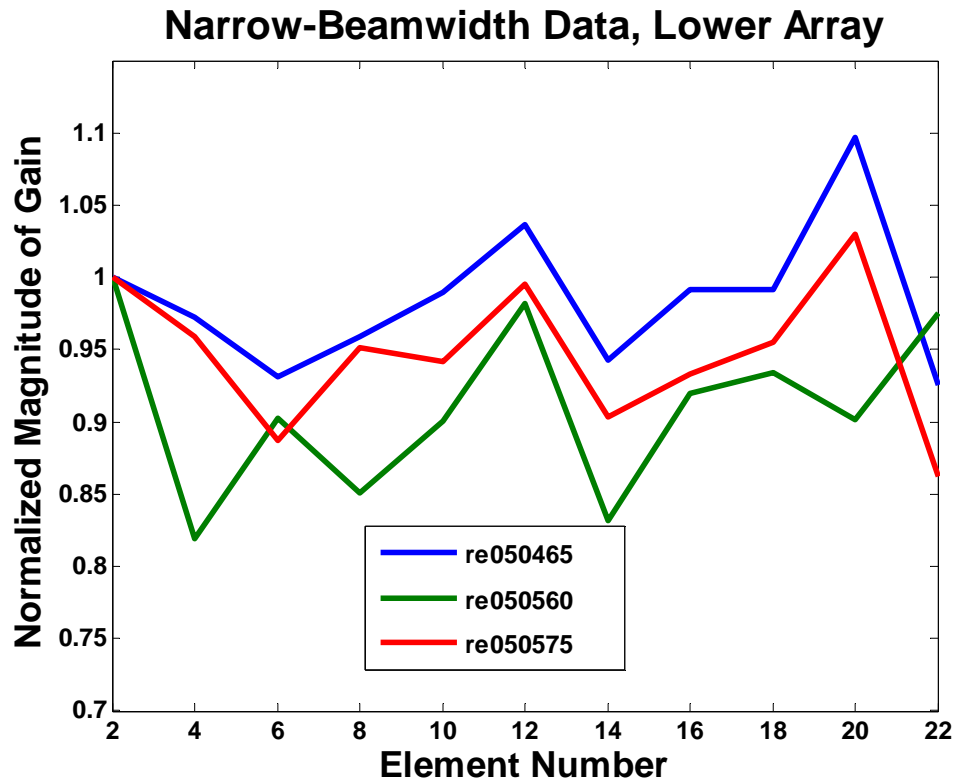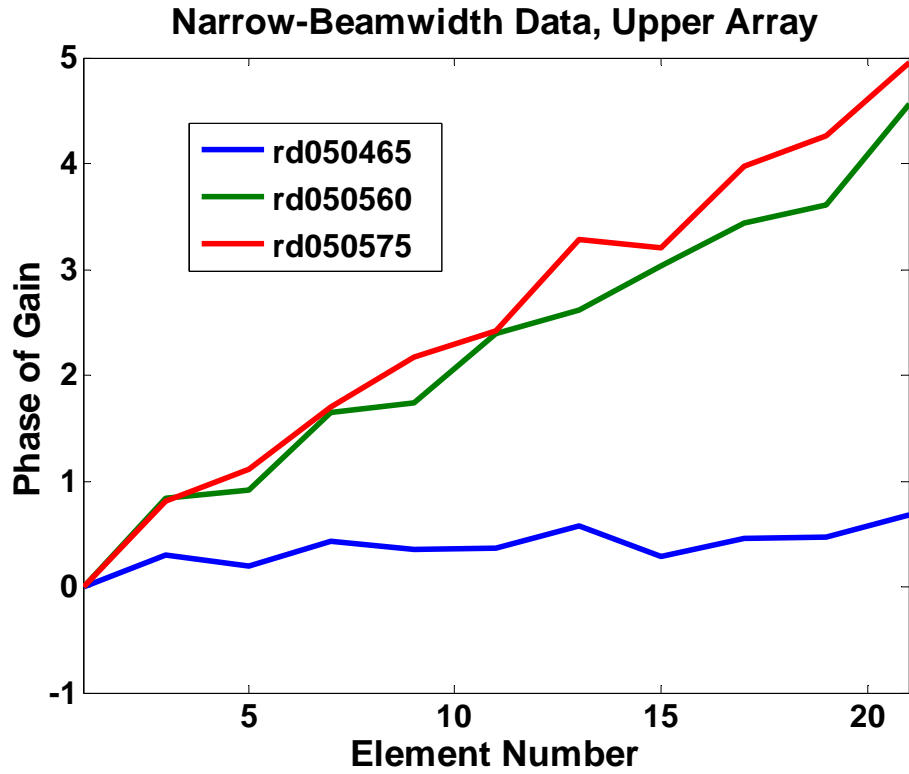
**Figure 3g: Estimated phase of complex gain, Narrow -beamwidth Data, Upper Array**
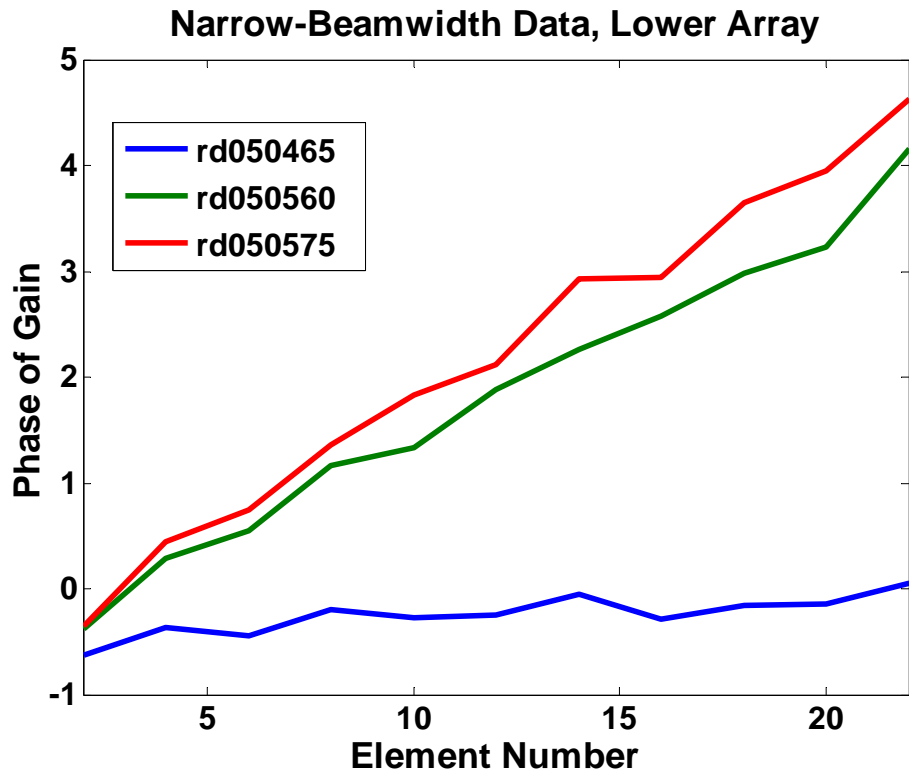


**Figure 3h: Estimated phase of complex gain, Narrow -beamwidth Data, Lower Array**

These result indicate that any MTI algorithm should first estimate and account for these calibration errors. For instance, the algorithm described in [14] would perform poorly without the above-mentioned global calibration. Moreover, to detect subtle and relatively weak moving targets, this simple global calibration is not sufficient. This problem is discussed next.

## 2.4. Local & Global Range-Doppler Dependent Calibration

We identify the globally-calibrated signal for the n-th receiver channel via

$$\hat{s}_n(t,u) = \frac{1}{\hat{a}_n} s_n(t, u - \hat{u}_n). \tag{7}$$

Consider the calibrated data for any two of the 22 receiver elements, e.g., n = 1 and n = 2. Let $\hat{S}_1(t,k_u)$ and $\hat{S}_2(t,k_u)$ be the slow-time (Doppler) Fourier transforms of $\hat{s}_1(t,u)$ and $\hat{s}_2(t,u)$, respectively. Provided that all 22 channels were calibrated via the global calibration method of Section III.C, the user could use the following statistic for MTI:

$$\hat{S}_d(t,k_u) = \hat{S}_2(t,k_u) - \hat{S}_1(t,k_u). \tag{8}$$

Let $f_2(x,y)$ and $f_1(x,y)$ be the SAR images that are formed from $\hat{S}_2(t,k_u)$ and $\hat{S}_1(t,k_u)$, respectively, via the method that was described in Section III.B. In this case, an equivalent MTI information can be constructed in the target scene reconstruction domain via

$$f_d(x,y) = f_2(x,y) - f_1(x,y). \tag{9}$$

Note that $f_d(x,y)$ is the SAR image that can be formed from $\hat{S}_d(t,k_u)$.

Due to various sources of errors (variations of the elements' radiation patterns in space, etc.), the global calibration of the 22 MCARM channels would not be sufficient to guarantee the success of the above MTI processing. In fact, in practice the MTI signatures are relatively weak, and can be dominated by even small miscalibrations.

To model these miscalibrations, we consider the two synthesized along-track MCARM channels in the $(t,k_u)$ domain or, equivalently, spatial $(x,y)$ domain. This is shown in Figure 4a.

14
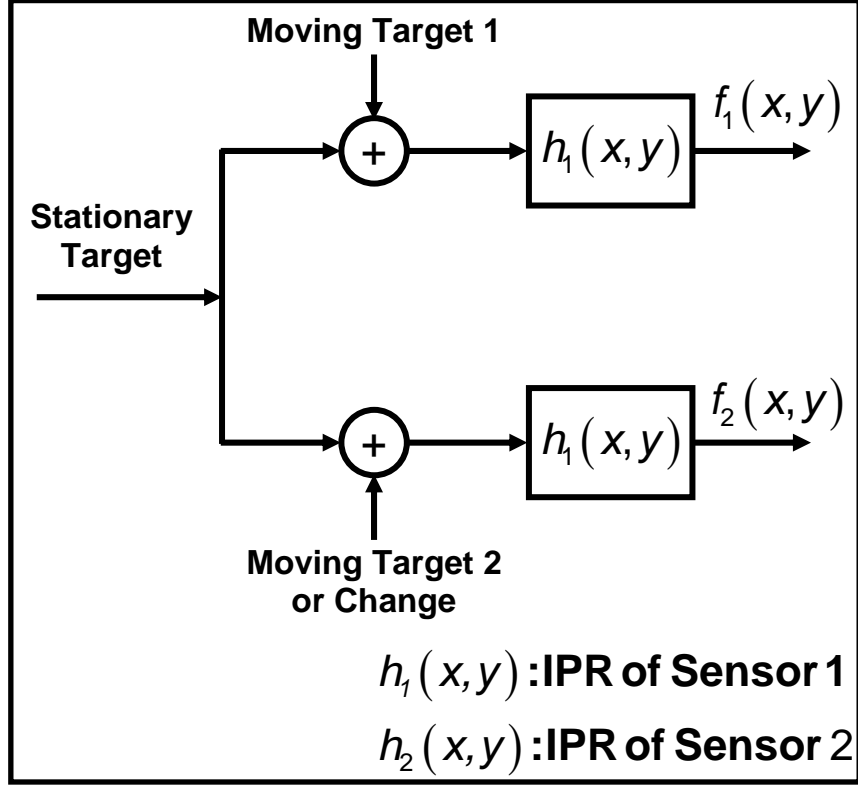
**Figure 4a: Signal model for dual channels of an along-track monopulse SAR system**

The calibration errors result in a spatially-varying point spread function (PSF) or Image Point Response (IPR) [12, Chapter 8]. However, within a small sub-patch of the target domain (e.g., a few hundred meters in both range and azimuth), the miscalibration PSF could be assumed to be spatially-invariant. For example, if $\hat{S}_{2m}(t,k_u)$ and $\hat{S}_{1m}(t,k_u)$ are the data for the m-th sub-patch that are centered at $t = t_m$ and $k_u = k_{um}$, we can relate these two signals (when there is no moving target) via the following 2D convolution:

$$\hat{S}_{2m}(t,k_u) \; = \; \hat{S}_{1m}(t,k_u) \otimes h_m(t,k_u), \tag{10}$$

where the 2D (complex) filter (PSF) function $h_m(t,k_u)$ is assumed to be unknown. Note that the filter function may also be represented as a spatially-varying PSF with respect to the center of the sub-patch via

$$h_m(t,k_u) = h(t,k_u;t_m,k_{um}). \tag{11}$$

A procedure to estimate the unknown filter function $h_m(t,k_u)$ via 2D adaptive filtering within a sub-patch is described in [11], [12, Chapter 8]. This procedure is referred to as Signal Subspace Processing (SSP) and is demonstrated in Figure 4b.

**2D Adaptive Filter**

**MTI or Change**

**Calibration Transfer Function:**

$$H(k_x, k_y) = \frac{H_2(k_x, k_y)}{H_1(k_x, k_y)}$$
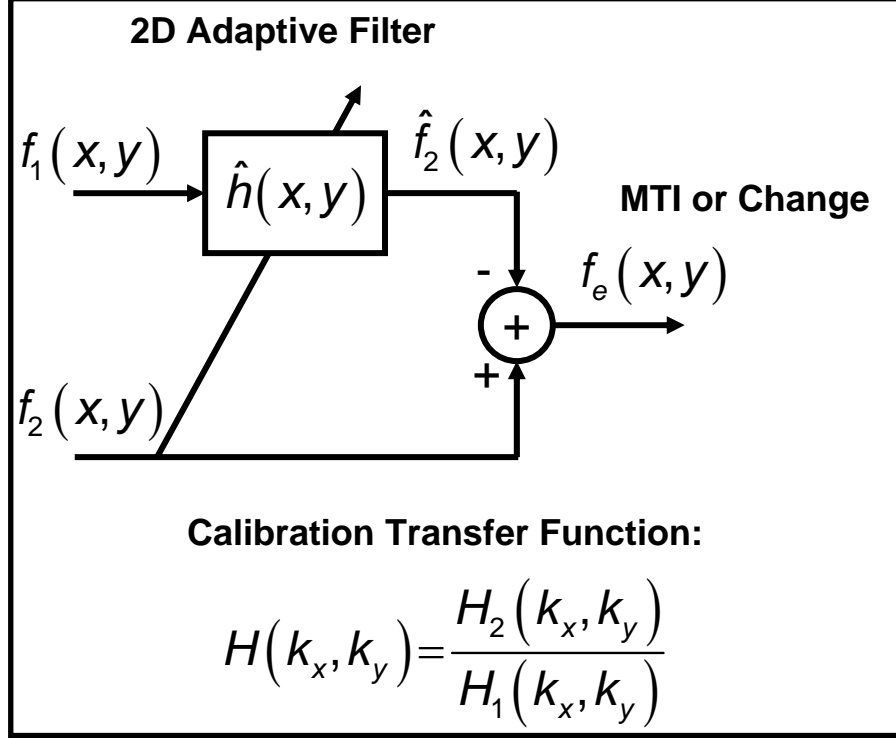
**Figure 4b: 2D Adaptive calibration of along-track monopulse SAR channels**

Let $\hat{h}_m(t, k_u)$ be the resultant estimated filter. Then, the MTI statistic for the m-th sub-patch is formed via:

$$\hat{S}_{dm}(t, k_u) = \hat{S}_{2m}(t, k_u) - \hat{S}_{1m}(t, k_u) \otimes \hat{h}_m(t, k_u). \tag{12}$$

We refer to the above as the Local Signal Subspace Difference (LSSD) image.

Our study of the along-track SAR data for MTI or change detection for various radar bands and SAR platforms has indicated that at times the Localized SSP algorithm not only removes the stationary targets but also performs a partial calibration with respect to a moving target at a sub-patch. This results in a weaker signature of the moving target in the LSSD image. To counter this problem, we hypothesized that since a radar system is a physical entity, the coefficients of the miscalibration filter/PSF $h_m(t, k_u)$ should not exhibit rapid fluctuations from one patch to its neighboring sub-patches for a stationary scene. A rapid change in a coefficient of the filter is most likely caused by adaptation of the SSP method to the signature of a moving target in that sub-patch.

Thus, the estimated filters that exhibit rapid fluctuations are not only unreliable but also are likely to be the ones that are adapting to moving target signatures and weakening their presence in the LSSD image. A simple remedy for this is to fit a low order 2D polynomial of the sub-patch location, i.e., $(t_m, k_{um})$, in the $(t, k_u)$ domain to each estimated filter coefficient. (The details of this scheme are beyond the scope of this report.) The resultant smooth spatially-varying filter function can then be applied to Channel 1 signal $\hat{S}_1(t, k_u)$. The outcome is then

subtracted form Channel 2 signal $\hat{S}_2(t,k_u)$ to form what we refer to as the Global Signal Subspace Difference (GSSD) image.

# 3. SYNTHESIS OF ALONG TRACK SAR CHANNELS

In the previous section, we presented the basic principles to interpret the data from a single receiver element of the MCARM system as a SAR signal. We then identified the data from two of the elements as the signal from an along track SAR system, and an adaptive method for 2D adaptive calibration of such a SAR system was presented for MTI purposes.

We now examine three methods for converting the data from all the 22 receiver elements of the MCARM system into a dual channel along-track SAR database.

## 3.1. MTI of 11-Element Average versus 11-Element Average with Maximum Along Track Baseline

In the first approach, we synthesize only one pair of along-track monopulse channels by dividing the globally range-Doppler invariant calibrated MCARM elements into two groups with 11 members each, and sum the members of each group. This method yields monopulse SAR channels with relatively high SNR values. Moreover, to improve the MTI performance, we synthesize the largest possible baseline in selecting members of the two groups.

For this purpose, we synthesize Channel 1 signal $\hat{s}_1(t,u)$ via summing the signals from Elements 1-11; i.e.,

$$\hat{s}_1(t,u) = \sum_{n=1}^{11} \frac{1}{\hat{a}_n} s_n(t, u - \hat{u}_n). \tag{13}$$

Channel 2 signal $\hat{s}_2(t,u)$ is constructed by summing the signals from Elements 12-22:

$$\hat{s}_2(t,u) = \sum_{n=12}^{22} \frac{1}{\hat{a}_n} s_n(t, u - \hat{u}_n). \tag{14}$$

One of the advantages of this approach is a fast construction of the MTI statistic. The main disadvantage of this technique is the information loss in averaging 11 elements (that is not a sufficient statistic).

## 3.2. Cumulative MTI of 1-Element versus 21-Element Average

As we mentioned before, the SAR-MTI method that is described in [14] performs poorly with the MCARM data. If one expands the matrix formulation in [14], it can be observed that the proposed approach is simply based on averaging the MTI statistic that is generated by paring one element versus the average of the other 21 elements. If the main shortcoming of that approach is *calibration*, the use of the global and local calibration algorithms could enhance the performance of the method in [14]. This is the basis of our second along track synthesis algorithm that is described next.

The second method that is studied involves synthesizing one channel of along-track monopulse SAR by averaging the globally range-Doppler invariant calibrated data from 21 elements of the MCARM; the 22nd element (after globally range-Doppler invariant calibration) is used as the second channel of the monopulse SAR system. We then perform SSP on the resultant two synthesized channels. This procedure is repeated using other 21-1 combinations (22

cases); the resultant 22 SSP differences (LSSD or GSSD) are accumulated as the final statistic for MTI.

Clearly, this procedure incorporates more information in constructing the final MTI statistic; it also utilizes some form of clutter/noise averaging (in the SSP differences) to improve SNR in the MTI. This is a more computationally expensive algorithm than the method described earlier (the SSP is performed 22 times); however, the 22 SSP-based pairings can be performed via a multi-processor.

### 3.3. Cumulative MTI of 1-Element versus 1-Element

The final approach in our study is based on using a pair of elements of the MCARM as the two channels of an along-track monopulse SAR system. We perform SSP on the resultant two channels. This step is then repeated using other pairs (231 cases); the resultant 231 SSP differences are added up to construct the information that is used for MTI. For this method, the coherent information in the individual elements is exploited in these 231 parings. Furthermore, since one anticipates more clutter and noise suppression in averaging the 231 SSP differences, this is the most promising approach for generating the MTI statistic.

In fact, when calibrating one element versus another element, a speckle pattern (noise) is generated due to subtle miscalibration at certain range and Doppler bins; however, when another pair is processed, the speckle noise miscalibraion at the same range-Doppler bin would most likely be different. This is known as *speckle averaging* effect in optics literature [15].

This method carries the highest computational burden. Yet, since the individual pairings are based on independent SSP operations that do not require the usage a significant amount of memory, the algorithm can be easily implemented on an on-board distributed memory multi-processor system.
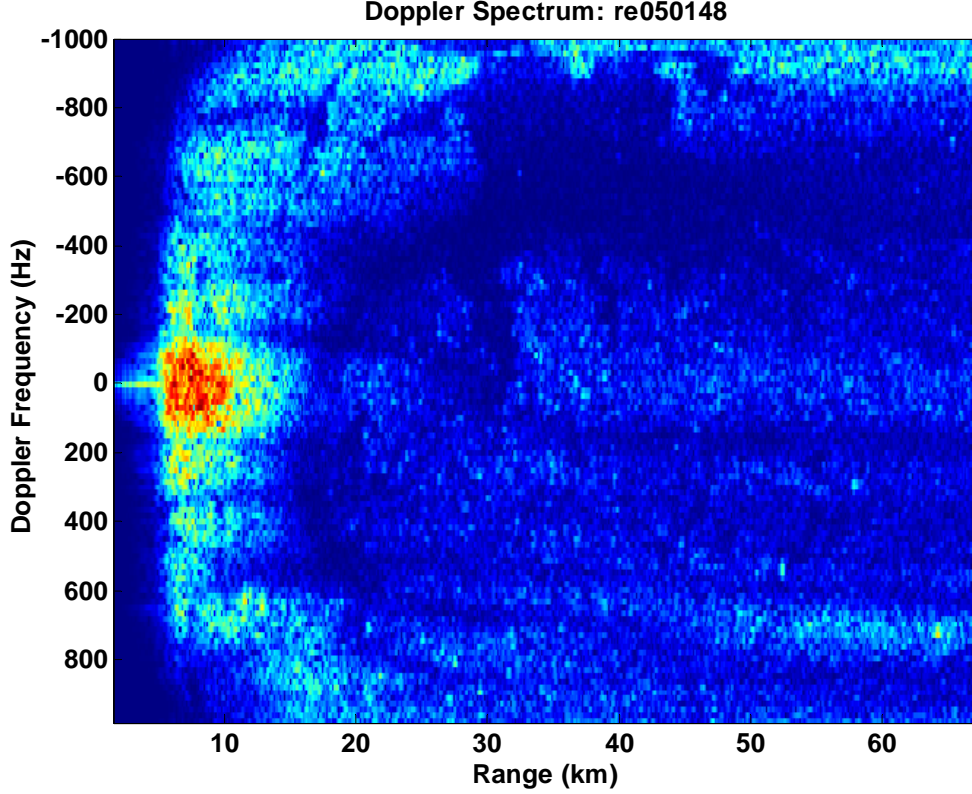
# 4. RESULTS

## 4.1. Wide-Beamwidth Data

Figure 5a and 5b, respectively, show the Doppler spectrum of a single element and the average of the first 11 elements (Synthesized Channel 1 as defined in Section III.A) for the wide-beamwidth RE-050148 MCARM data).
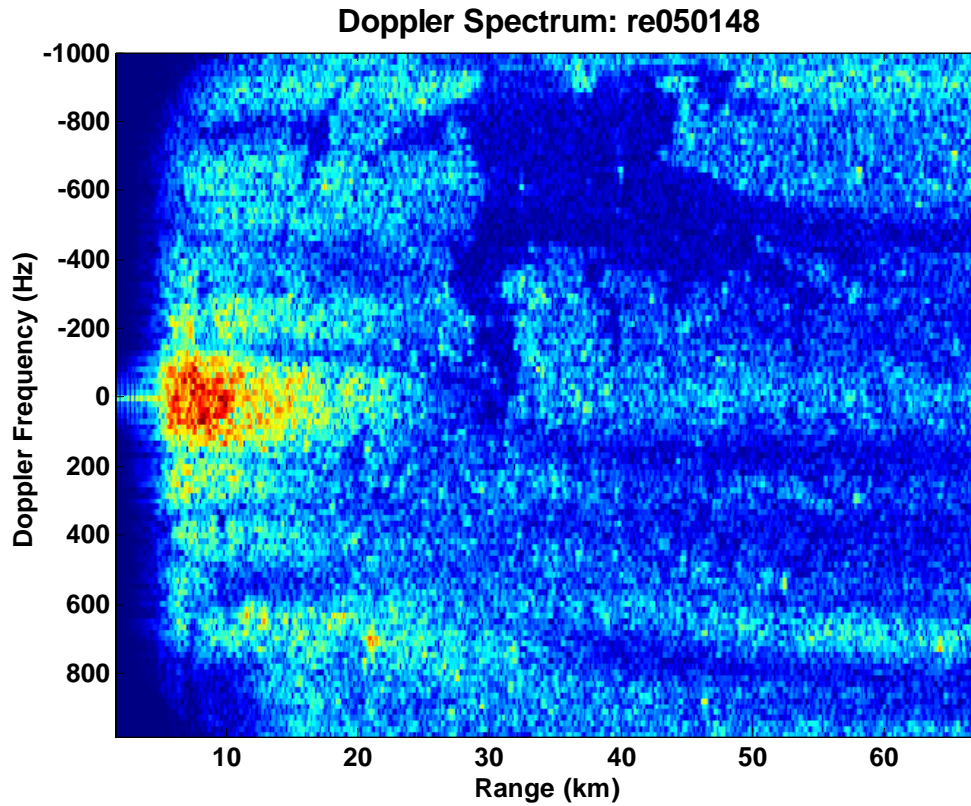


**Figure 5a: Doppler Spectrum: Synthesized Channel 1 for Wide-Beamwidth re050148 Data**

**Figure 5b: Doppler Spectrum: Synthesized Channel 1 (Average 11 Elements) for Wide-Beamwidth re050148 Data**

As we mentioned earlier, the wide-beamwidth databases were collected around a bay area (land and water); a Moving Target Simulator (MTS) was also present. We used the sum of 11 elements with globally range-Doppler invariant calibration of Section II.C to generate Figure 5b; this cumulative Doppler spectrum provides a more informative (better SNR) image than the one that is obtained from a single element in Figure 5a for *stationary* targets.

Figure 6a is the Doppler spectrum of a single element around the signature of the MTS that is approximately located at the range of 46.2 km and the Doppler band of [-1,0] kHz; the first two simulated moving targets are visible in this figure.
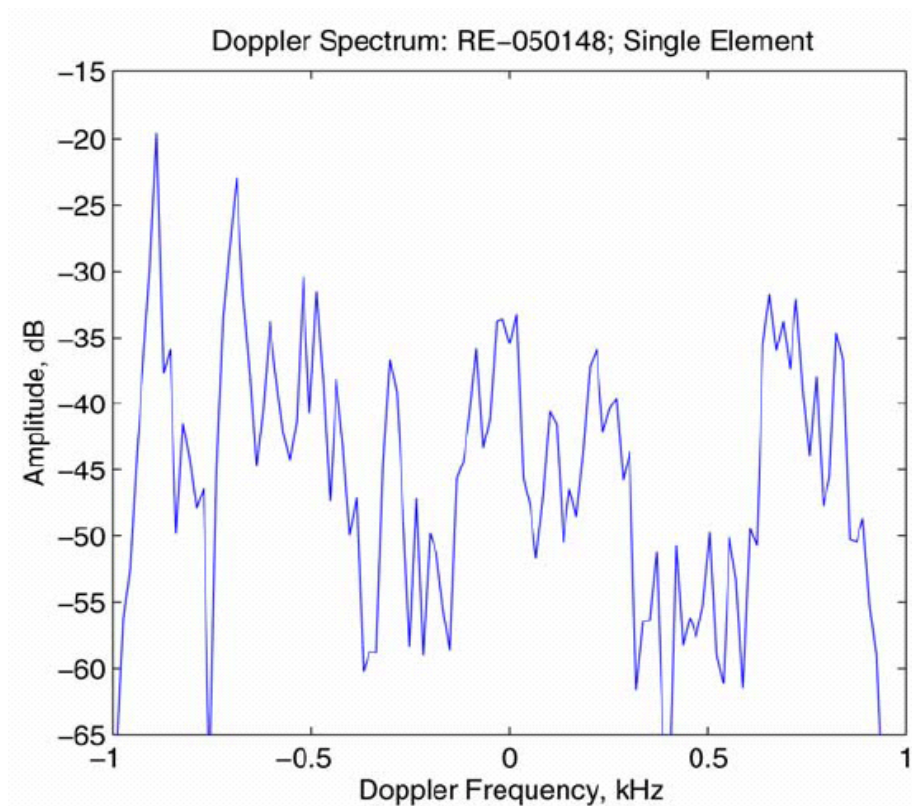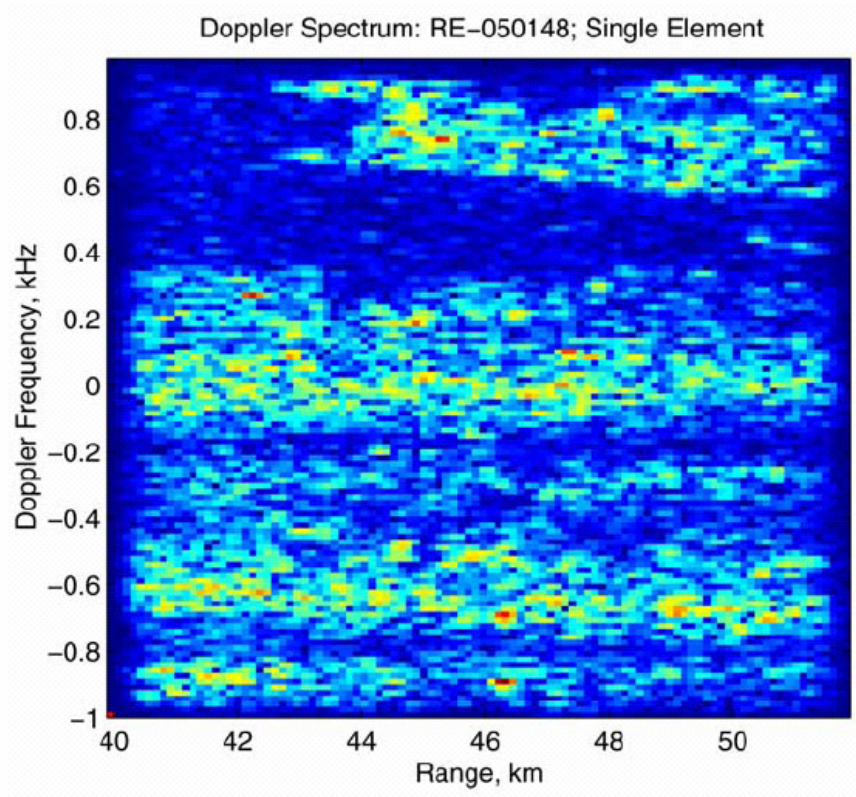
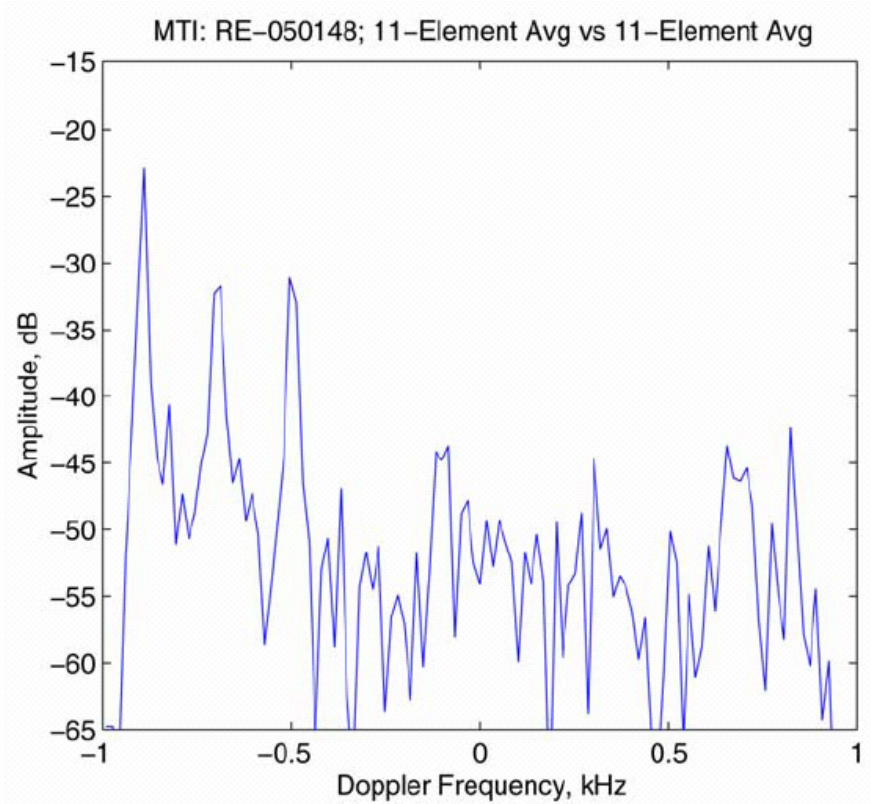**Figure 6a:  Single Element for Wide-Beamwidth re050148 Data around MTS**

Figure 6b is the Doppler spectrum of the same area that is obtained with the sum of all 22 elements with globally range-Doppler invariant calibration (i.e., a zoomed version of Figure 5 in which 11 elements are combined). Note that the stationary scene appears more prominent while the MTS signatures have eroded. This should be anticipated since the global range-Doppler invariant calibration of Section II.C assumes a stationary target scene model, and its goal is to reinforce the signatures of such targets.

Doppler Spectrum: RE-050148; Sum of 22 Elements



Doppler Spectrum: RE-050148; Sum of 22 Elements
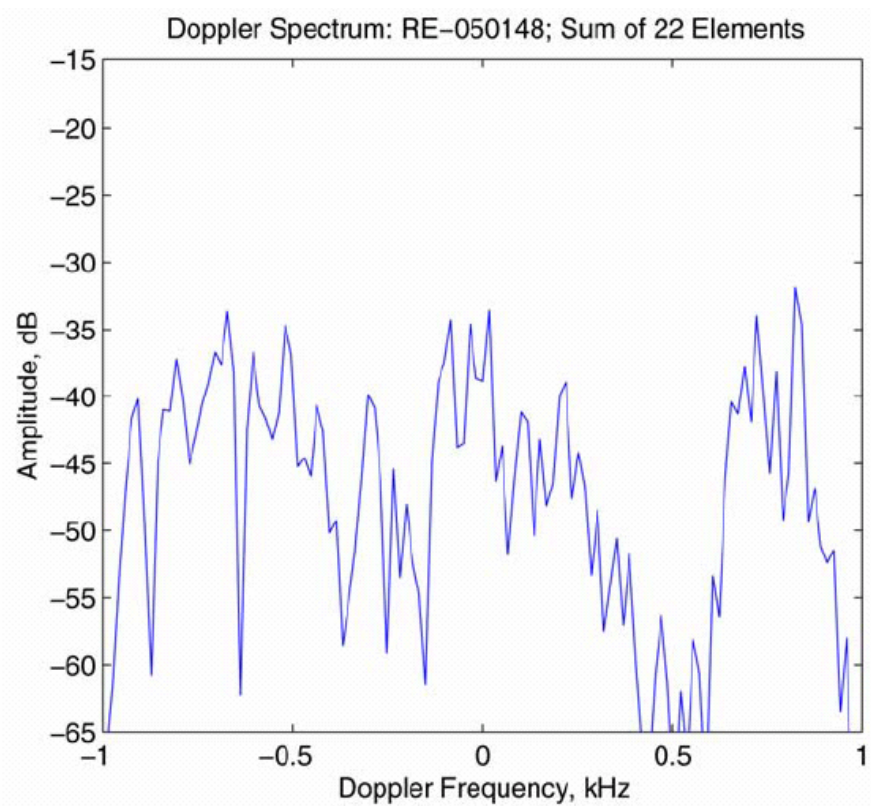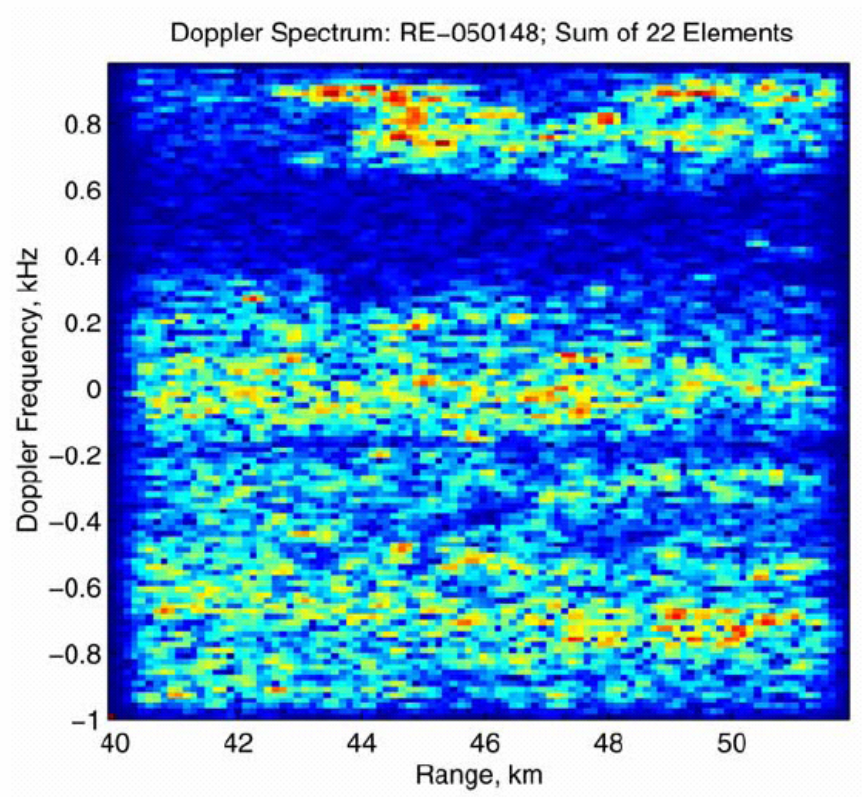
**Figure 6b: Sum of 22 Elements for Wide-Beamwidth re050148 Data around MTS**

Next we examine the MTI results for the area in Figure 6a (or 6b) using the range-Doppler varying calibration algorithms of Section III. Figure 6c shows the MTI results using the 11-element average versus 11-element average with the largest along-track separation baseline of Section III.A; Figure 6d is the MTI for the cumulative 1-element versus 21-element average of Section III.B; and, Figure 6e is the MTI outcome for the cumulative 1-element versus 1-element algorithm of Section III.C. For all three methods, the GSSD performed better than the LSSD (see Section II.D); the MTI results that are shown in Figures 6c-e are the GSSD images.
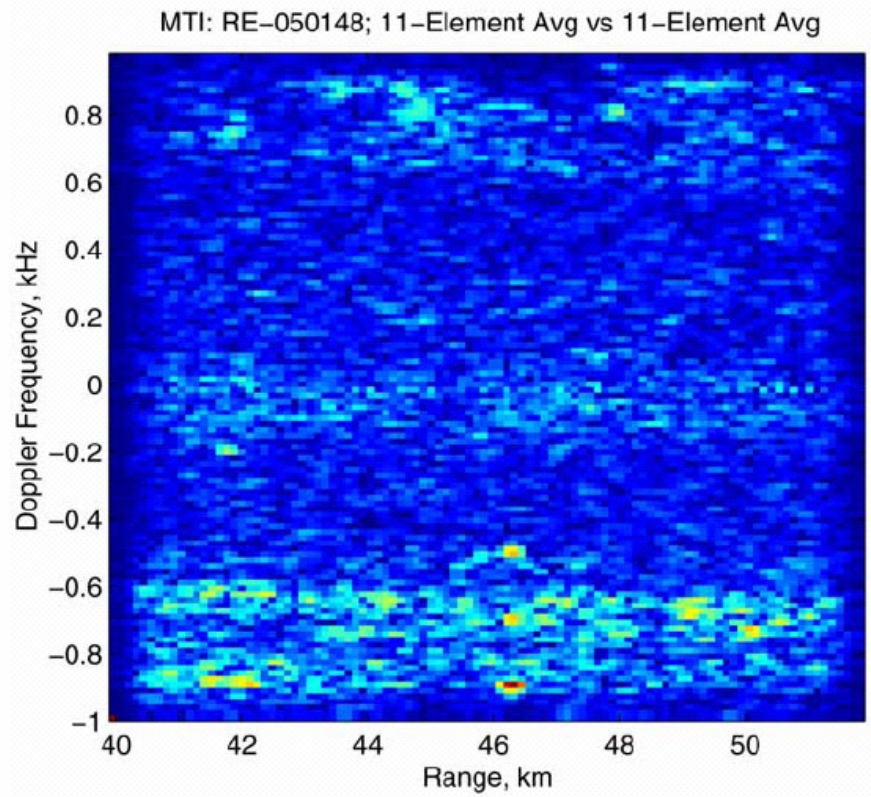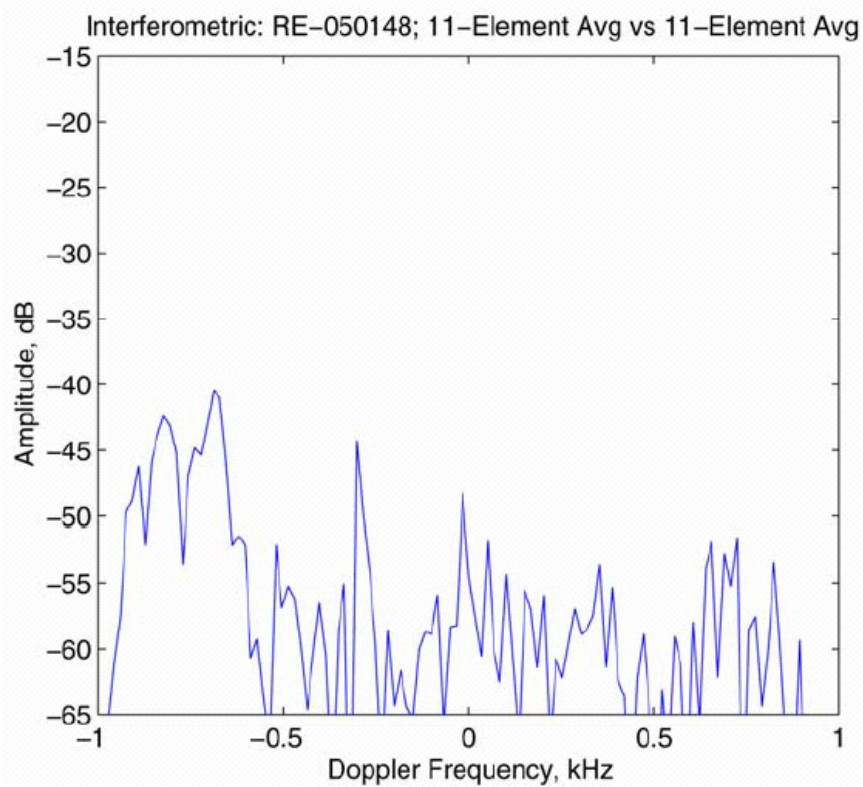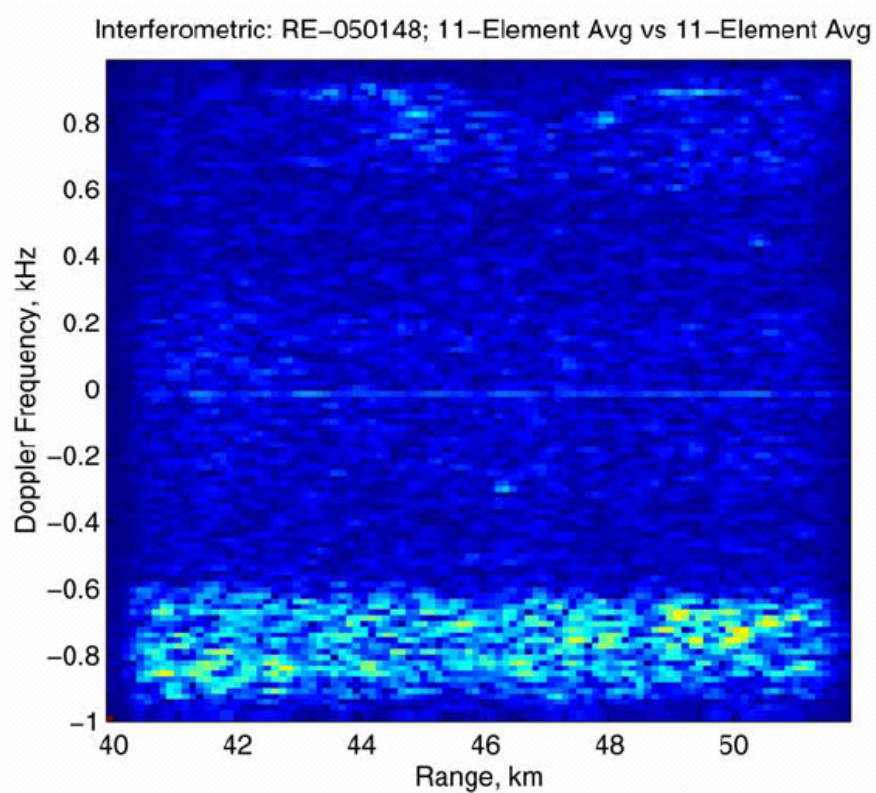
**Figure 6c: MTI, 11-Element Average vs. 11-Element Average for Wide-Beamwidth re050148 Data around MTS**
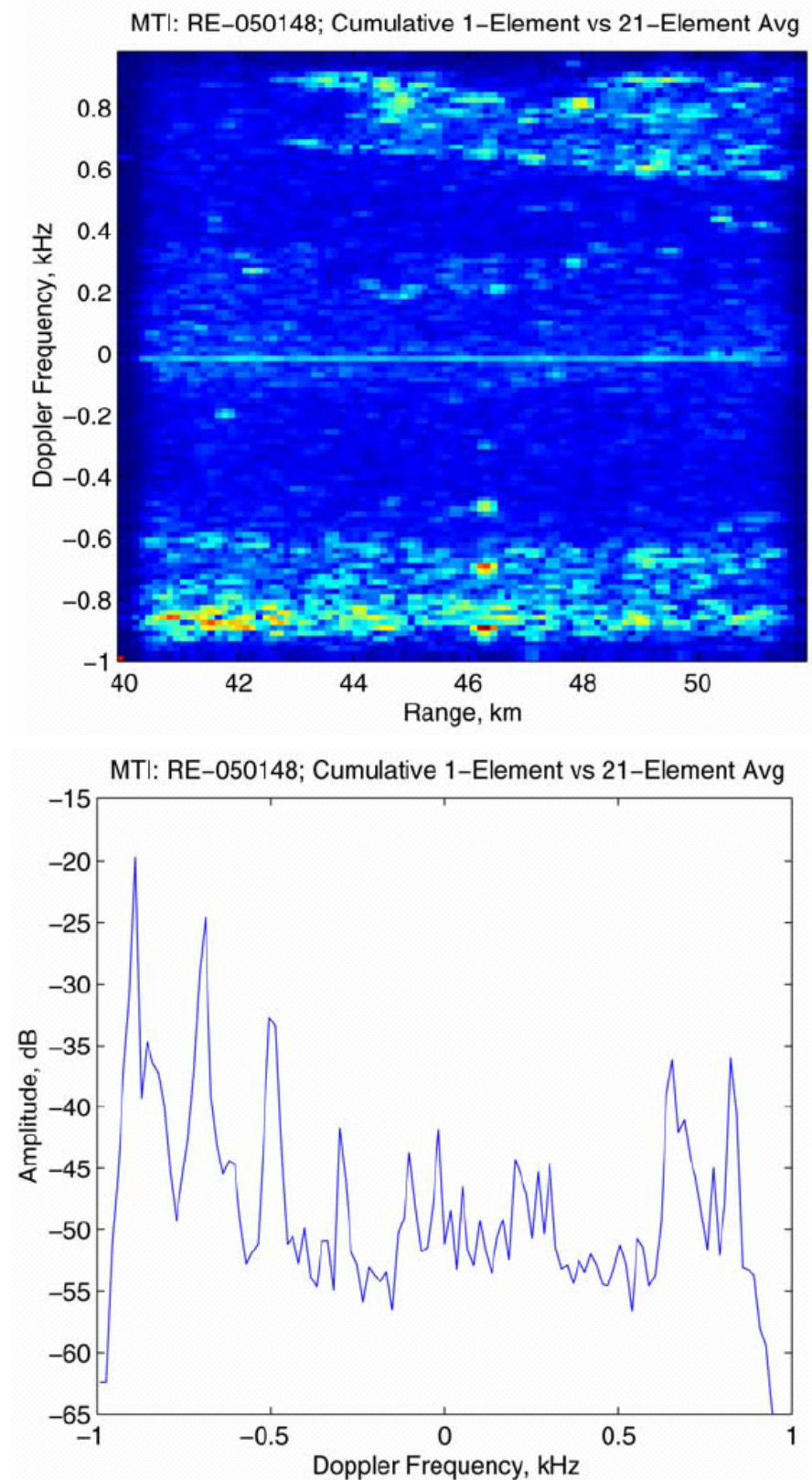
**Figure 6d: MTI, Cumulative 1-Element vs. 21-Element Average for Wide-Beamwidth re050148 Data around MTS**

**Figure 6e: Interferometric, 11-Element Average vs. 11-Element Average for Wide-Beamwidth re050148 Data around MTS**

By comparing the MTI images in Figures 6c-e, the cumulative 1-element versus 1-element algorithm of Section III.C (Figure 6e) seems to provide the best GSSD outcome in which a fairly uniformly-distributed speckle signature with prominent MTS signatures (particularly the ones with larger Doppler frequencies) are observable.

To test the validity of MTI extraction based on separation of two channels in the along-track domain and their calibration, we perform a study in which Channel 1 is synthesized using the sum of the 11 upper elements (Modules 2, 4, 6, 8, …), and Channel 2 is synthesized via the sum of the 11 lower elements (Modules 3, 5, 7, 10, …) of the MCARM (see Figure 1). This scenario corresponds to a (theoretical) zero size along-track baseline and, thus, the SSP algorithm should null not only the stationary targets but also the moving targets. (This type of airborne radar data collection is used for determining elevation in SAR systems via interferometric processing of the two channels.) Figure 6f shows the resultant GSSD in which the two channels are approximately nulled at all range and Doppler points. (It is not clear why the GSSD shows a relatively stronger signature along a negative Doppler band than the positive Doppler band.)

The results in Figure 7 correspond to the SAR interpretation and imaging of the MCARM data (Section II.B). Figure 7a is the SAR image that is produced from Figure 5 (Doppler spectrum). Note that the radar beam shows energy within a beam angle of near 150 degrees. Figure 7b is the SAR-MTI image of the scene in Figure 7a. Figure 7c is a close-up of the images in Figures 7a-b. The zoomed image is a portion of the reconstruction at the edge of the beam that shows a bay area near the Baltimore airport. In the top SAR image, the red patches correspond to the (stronger) ground clutter; the dark areas (around range 15 km to 35 km) are mostly the waterways in the bay area. The bottom SAR-MTI image indicates a significant reduction in the signature of the ground clutter (more than 35 dB). Meanwhile the MTI shows various targets (white signatures) particularly on the waterways in the bay area. We should point out that these signatures are present in the SAR image of Figure 7a (the upper image in Figure 7c), though they are very weak.

**SAR Reconstruction**
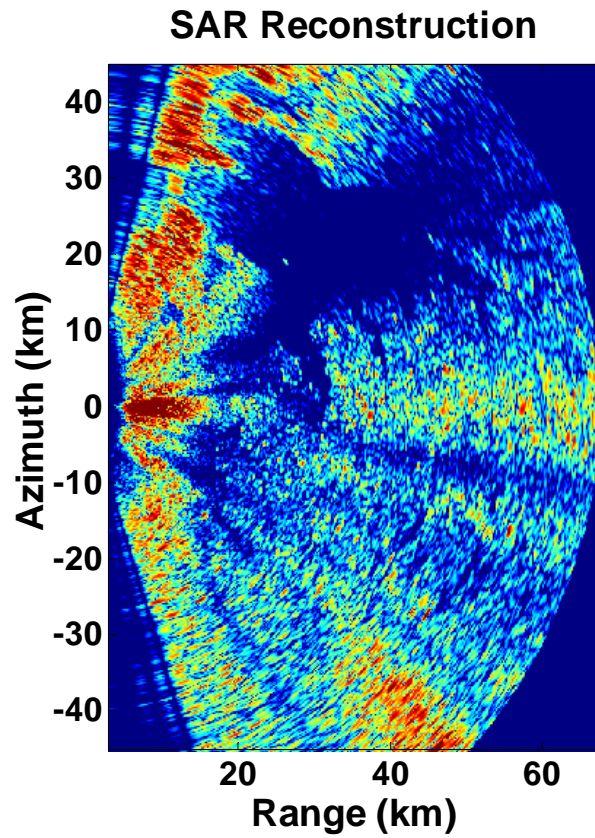


**Figure 7a: SAR Reconstruction, Synthesized Channel 1 (Average 11 Elements) for Wide-Beamwidth,b re050148 Data**

## SAR-MTI Reconstruction
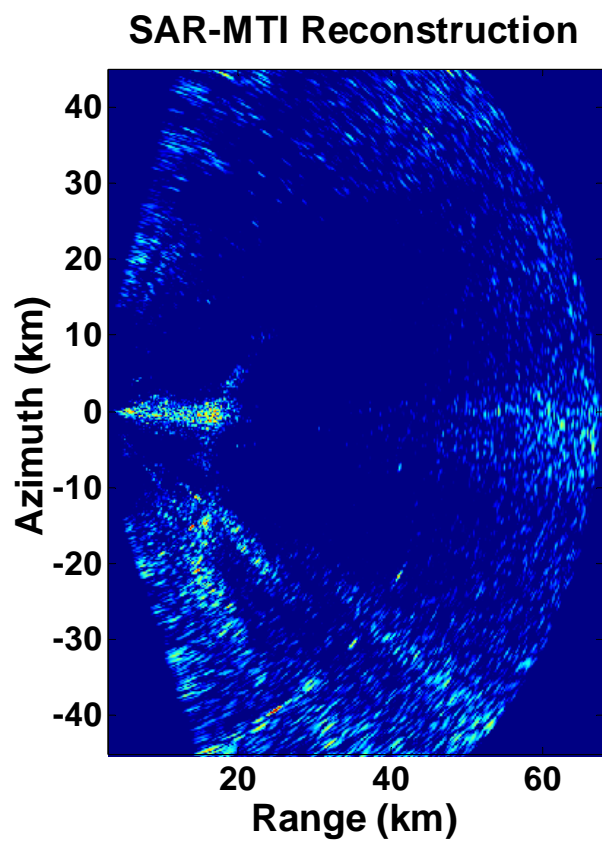


**Figure 7b:  SAR Reconstruction, MTI for Wide-Beamwidth re050148 Data**

## SAR Reconstruction
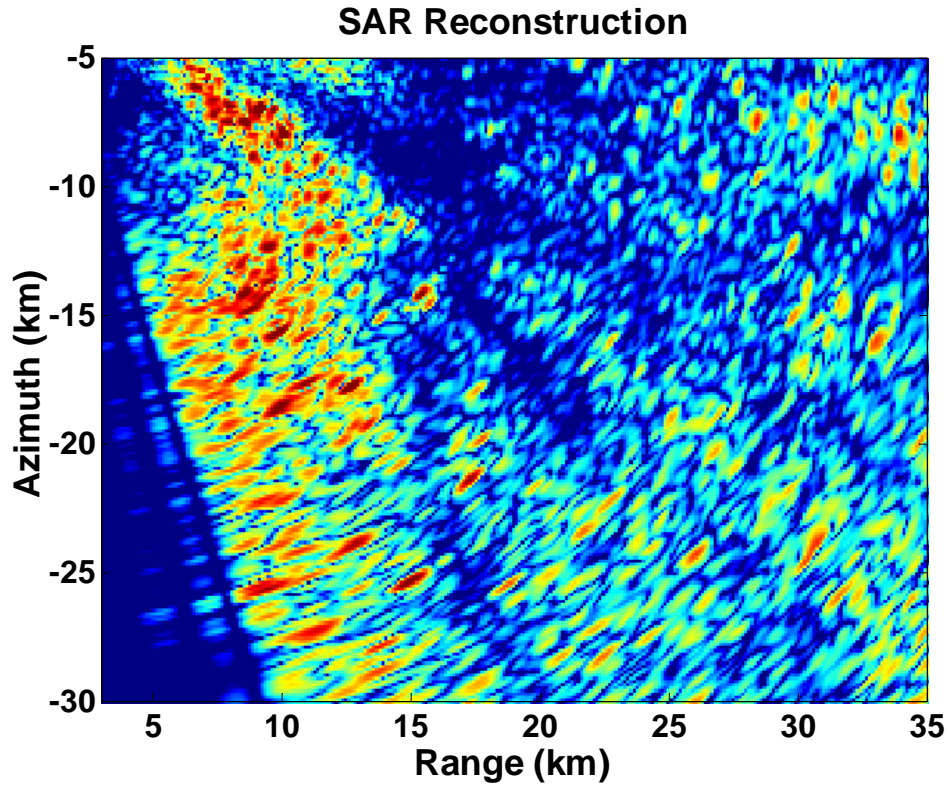


**Figure 7c: Zoomed version of Figure 7a around a Water Channel**

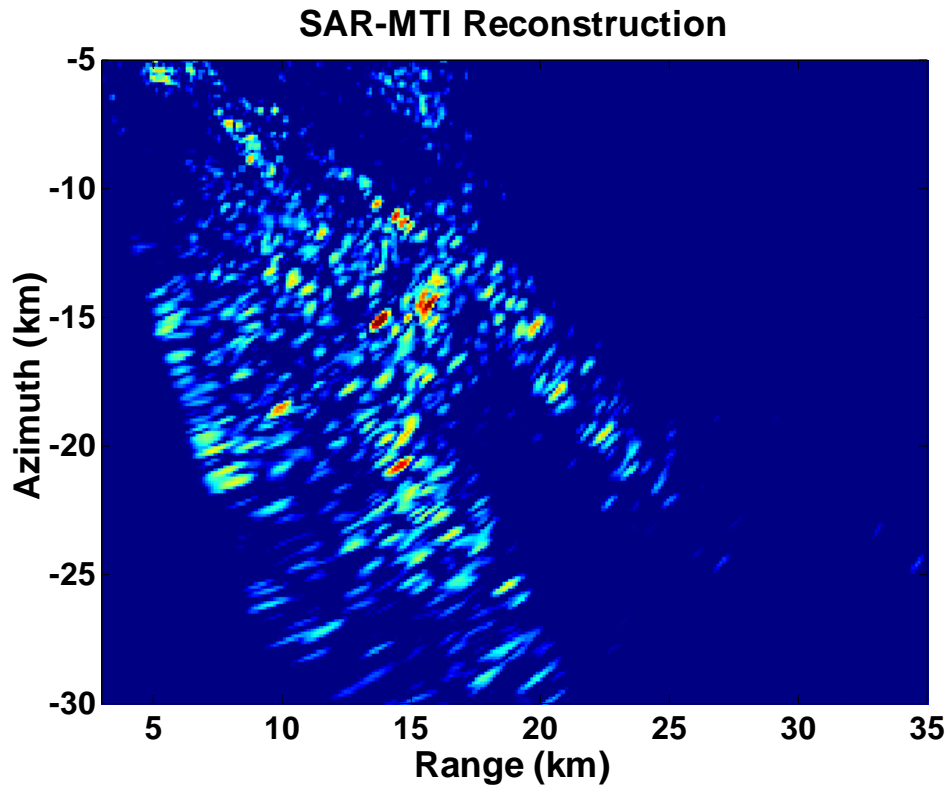## SAR-MTI Reconstruction



**Figure 7d: Zoomed version of Figure 7b around a Water Channel**

32

## 4.2. Narrow-Beamwidth Data

Next we examine examples from the narrow-beamwidth databases. Figure 8a is the Doppler spectrum of the database RD-050575; Figure 8b is its SAR spatial image. Note that the SAR image in Figure 8b shows a narrower radar beamwidth (about 30 degrees as opposed to 150 degrees for the wide-beamwidth SAR image in Figure 7a) with significant sidelobes; the radar beam also appears to be tilted by approximately 4-5 degrees.
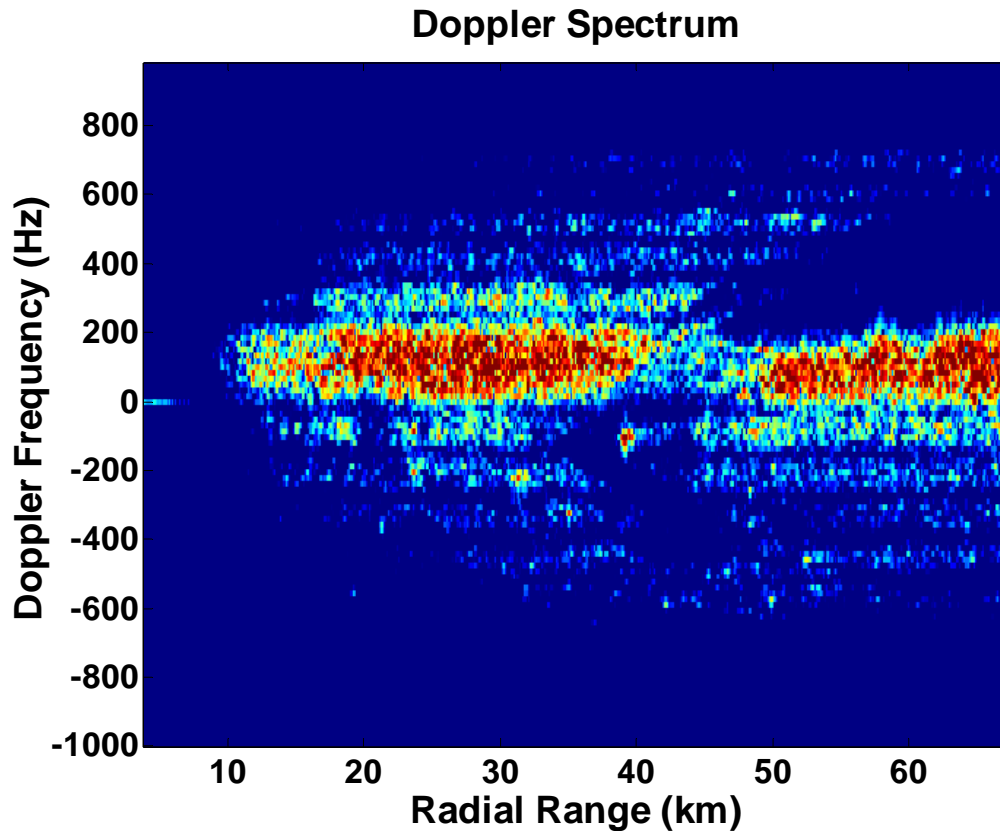
**Doppler Spectrum**



**Figure 8a: Doppler Spectrum, Synthesized Channel 1 (Average 11 Elements) for Narrow-Beamwidth rd050575 Data**

## SAR Reconstruction
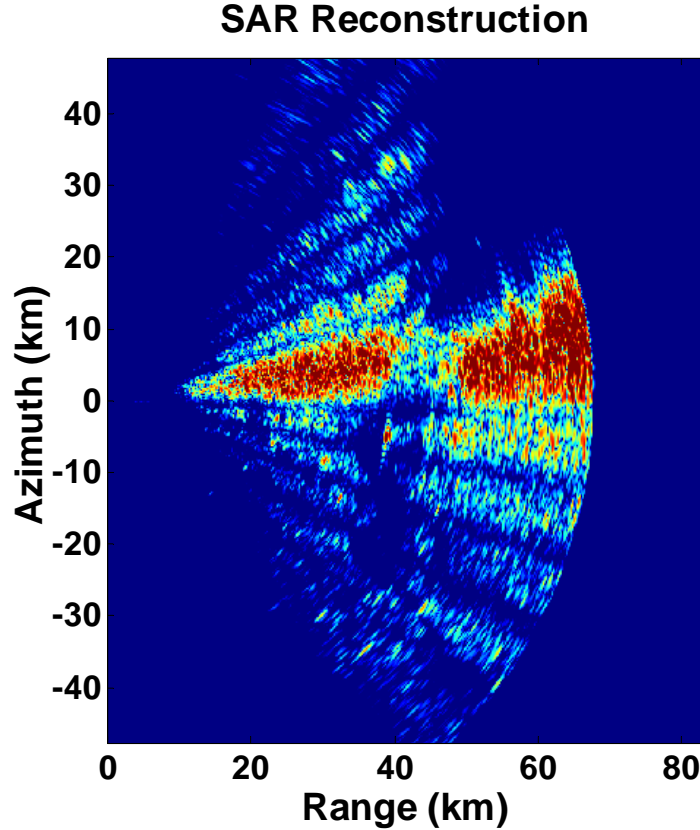


**Figure 8b:  SAR Reconstruction, Synthesized Channel 1 (Average 11 Elements) for Narrow-Beamwidth rd050575 Data**

The top image in Figure 9 is a close-up of the SAR image in Figure 8b in  a region that is around the mainlobe of the radar beam. The bottom portion of Figure 9 is the SAR-MTI image of the close-up area that is generated from the LSSD data (see Section II.D) using the 11-element average versus 11-element average with the largest along-track separation baseline of Section III.A; the LSSD of this algorithm appears to provide a better clutter (stationary target) suppression than the GSSD (not shown here) and the LSSD/GSSD MTI results for the speckle averaging algorithms of Sections III.B and III.C. This is contrary to our observations for detecting the MTS in the wide-beamwidth data.

## SAR Reconstruction
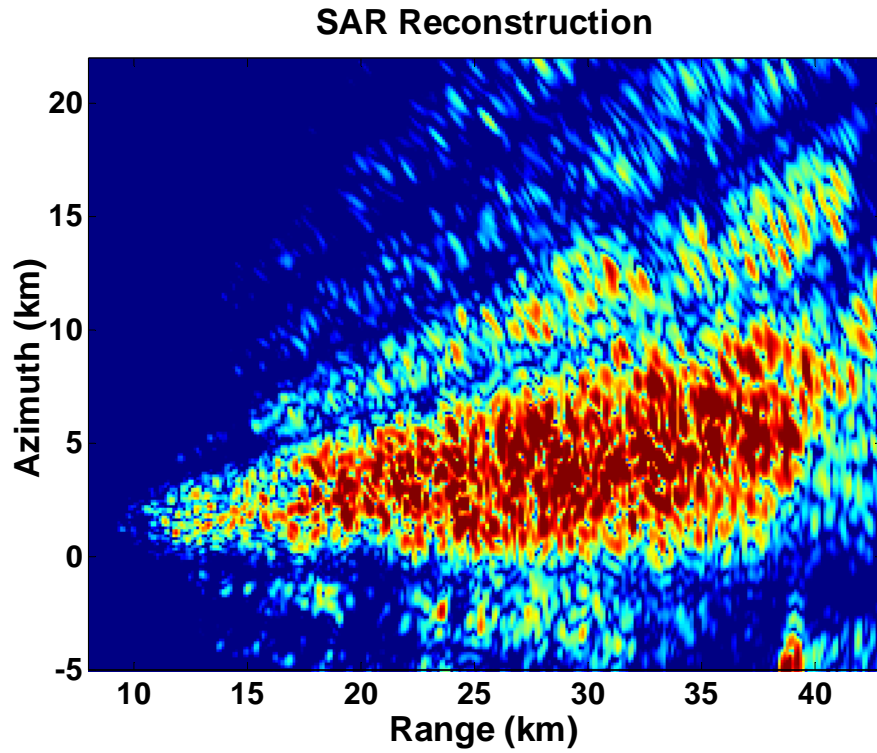


**Figure 9a: Narrow-Beamwidth rd050575 Data: SAR reconstruction around the radar mainlobe (highway area)**
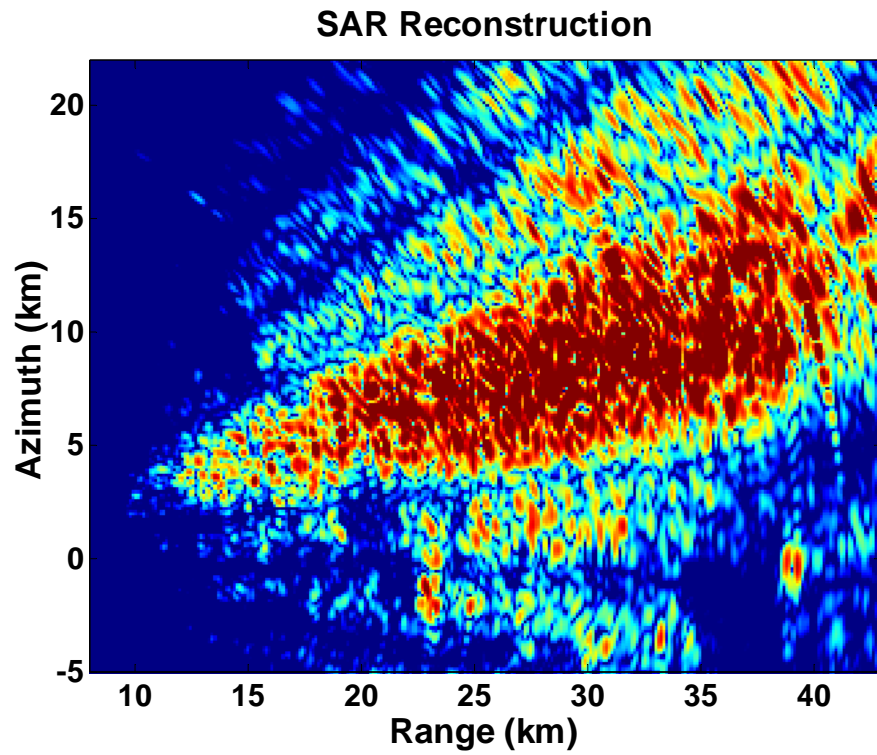
## SAR-MTI Reconstruction
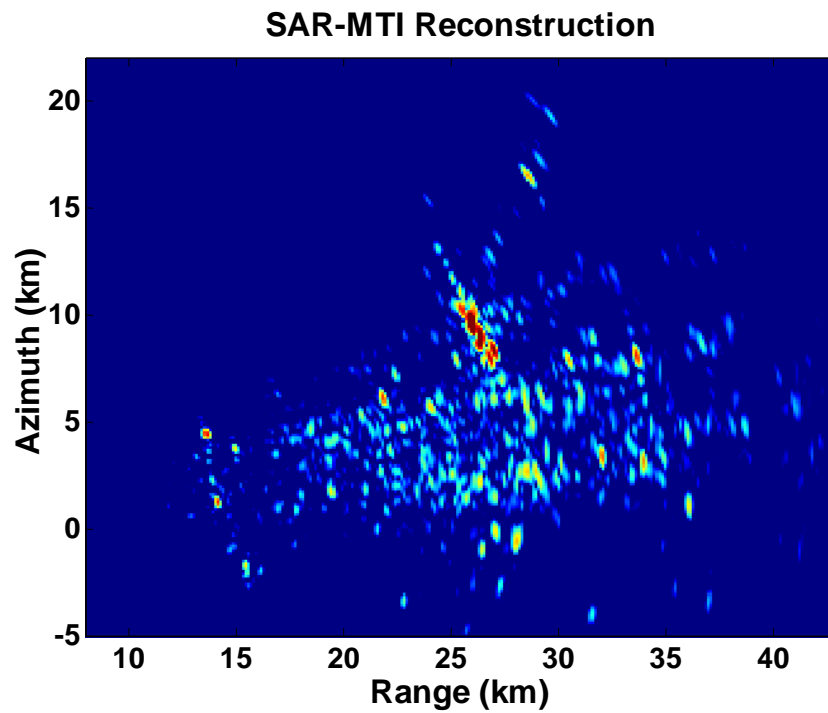


**Figure 9b: Narrow-Beamwidth rd050575 Data, SAR-MTI image around the radar mainlobe (highway area)**

This phenomenon may be rationalized based on the following. The imaging area in Figure 9 is composed of various highways with moving automobiles on them. These automobiles are relatively small box-looking structures whose radar signature may be *detectable/observable* by the radar A/D hardware (in the presence of a strong ground clutter return) at only close to 0, 90, 180, and 270 aspect angles. Moreover, the speed of a typical moving automobile is less than 35 m/sec (70 mph). For the L-band MCARM radar traveling at the speed of about 125 m/sec with an along-track baseline separation of .1 m to 1 m, the likelihood of detecting subtle phase changes of a moving automobile (i.e., MTI information) in such a heavy ground clutter by comparing the signals of two individual elements is unlikely. Thus, the 11-element average versus 11-element average algorithm of Section III.A, that is designed to improve SNR with the largest along-track separation baseline, should be the logical choice for this scenario. (Note that the MTS signatures in the wide-beamwidth data are fairly strong and visible in a single element data of Figure 6a.)

The improved performance of the LSSD over the GSSD could be due to the order of the 2D polynomial (21: 4-th order in both range and Doppler domains with cross terms) that we used. It is likely that the radar beam phase variations (calibration errors) are more fluctuating for the narrow-beamwidth (focused) radar beams of Figures 9-11 than the wide-beamwidth data of Figure 6. In this case, modeling the range and Doppler varying miscalibration filter/PSF $h_m(t, k_u)$ (see Section II.D) via a low order polynomial is not sufficient for the narrow-beamwidth data. (Increasing the order of the 2D polynomial improves the GSSD results since in the case of using a high order model for $h_m(t, k_u)$, the GSSD becomes the LSSD.)

Figures 10 and 11 show similar results from two other narrow-beamwidth snapshots of the MCARM for the same flight. For these cases, the radar beam was tilted by about 12 degrees. By comparing the SAR-MTI (bottom) images of Figures 9, 10 and 11, one can see changes in the coordinates of the moving automobiles that possess different velocities. Moreover, it is believed that the airborne saber liner was located at a wrap-around (ambiguous) range of 30 km. (Unfortunately, accurate ground-air truths are not available.) An interesting phenomenon can be seen in the SAR-MTI image of Figure 11. This image shows a set of *flashing* moving targets that are *lined up* at an angle of 20 degrees with respect to the radar boresight; then a line of flashing moving targets that is approximately perpendicular to the first line is visible at the range of about 30-32 km. This corresponds to a scenario of two perpendicular highways with automobiles that are at aspect angles of close to 0 (or 180) degrees on one highway, and automobiles that are at aspect angles of close to 90 (or 270) degrees on the other highway.

## SAR Reconstruction



**Figure 10a:  Narrow-Beamwidth rd050560 Data, SAR reconstruction around the radar mainlobe (highway area)**

## SAR Reconstruction
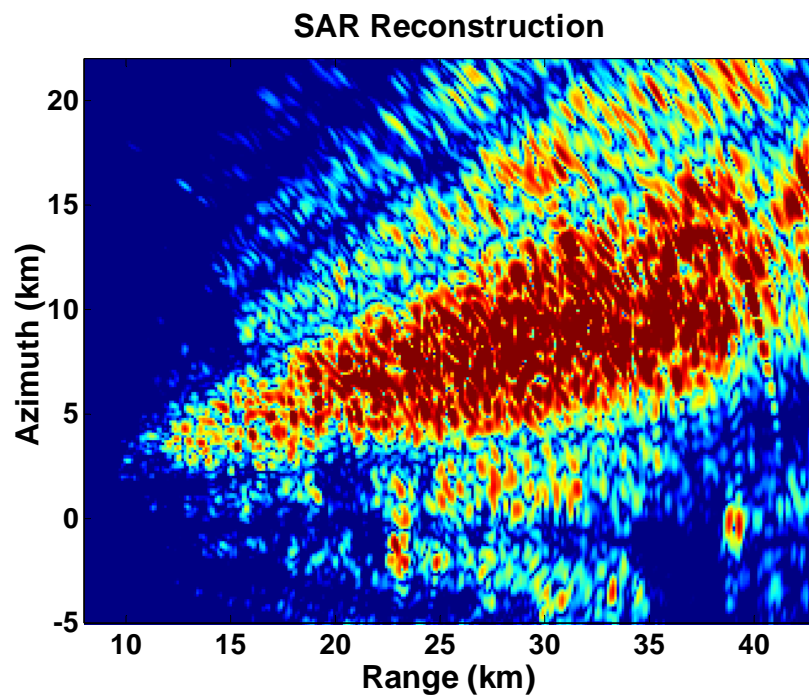


**Figure 10b:  Narrow-Beamwidth rd050560 Data, SAR-MTI image around the radar mainlobe (highway area)**

## SAR Reconstruction
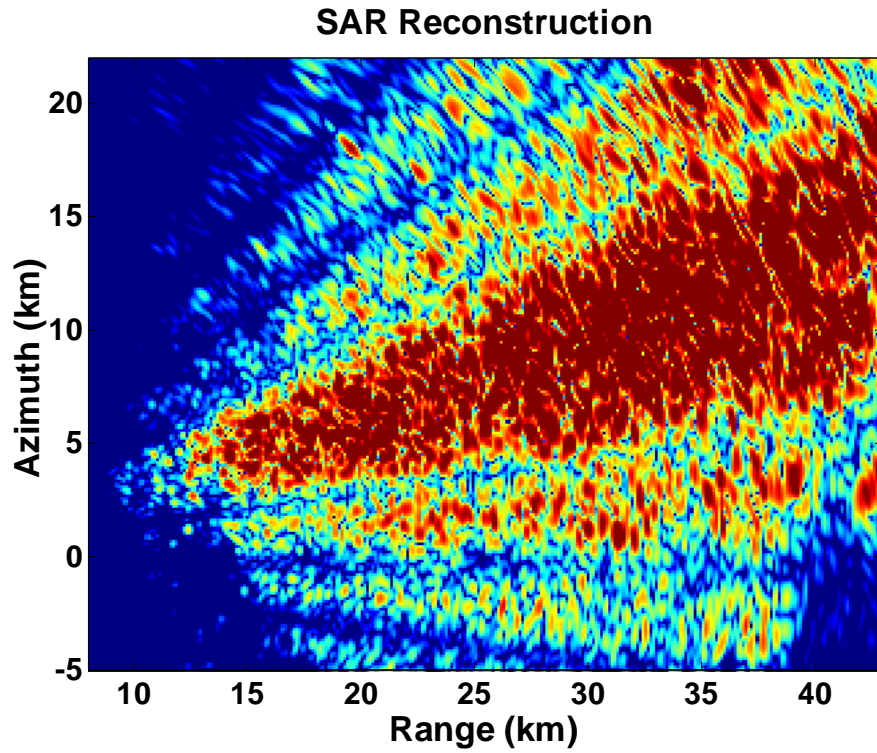


**Figure 11a:  Narrow-Beamwidth rd050614 Data, SAR reconstruction around the radar mainlobe (highway area)**

## SAR-MTI Reconstruction
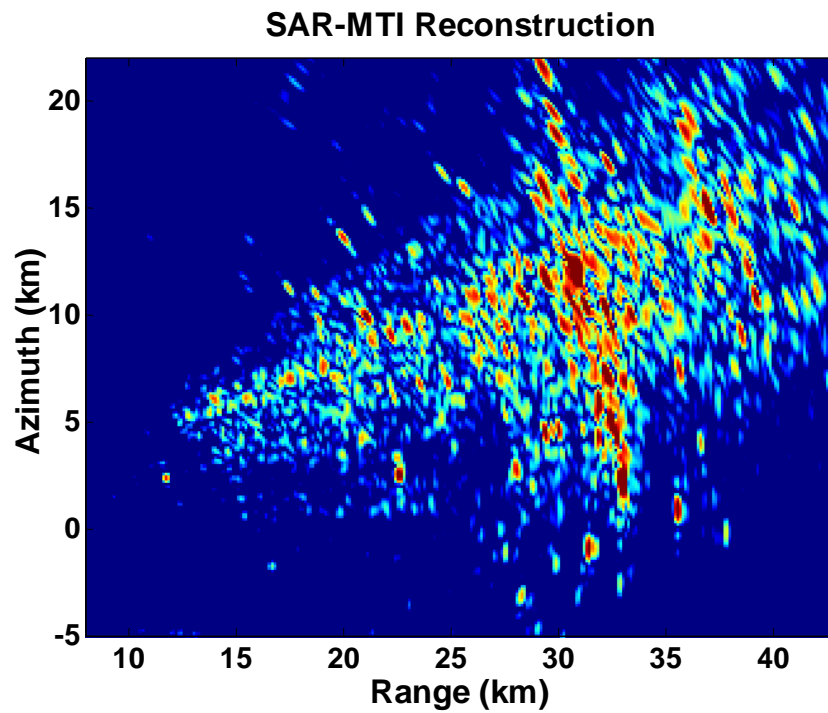


**Figure 11b:  Narrow-Beamwidth rd050614 Data, SAR-MTI image around the radar mainlobe (highway area)**

# 5. SUMMARY

This report examined the processing of multi-channel airborne radar data in the framework of the principles of SAR and its associated imaging and along-track monopulse MTI processing. The study of narrow-beamwidth and wide-beamwidth data revealed the strengths and weaknesses of three algorithms for combining the data from the available 22 channel of the MCARM system as well as with the global versus local (GSSD vs LSSD) range-Doppler varying modeling of the calibration filter.

# 6. REFERENCES

1. "Multi-Channel Airborne Radar Measurement (MCARM)", See https://watto3.deepthought.rl.af.mil/MCARM/.

2. W.L. Melvin et al., "Assessment of Multi-channel Airborne Radar Measurements for Analysis and Design of Space-Time Processing Architectures and Algorithms," *Proc. IEEE Natl. Radar Conference*, Ann Arbor, MI, pp. 130-135, May 1996.

3. W. L. Melvin and B. Himed, "Comparative Analysis of Space-Time Adaptive Algorithms with Measured Airborne data," *Proc. 1996 ICSPAT Conference*, Boston, October 1996.

4. W.L. Melvin and M.C. Wicks, "Improving practical space-time adaptive radar," *Proc. IEEE Natl. Radar Conference*, pp. 48-53, May 1997.

5. B. Himed and W. L. Melvin, "Analysis of Reduced-Dimension Space-Time Adaptive Processors using Monostatic MCARM Data," *Proc. 1997 ISDSP Conference*, London, July 1997.

6. B. Himed and W. L. Melvin, "Analyzing Adaptive Space-Time Processors Using Measured Data," *Proc. 31-st ASILOMAR Conf. on Signals, Systems and Computers*, Monterey, CA, November 1997.

7. B. Himed, ``MCARM/STAP Data Analysis," Final Technical Report, AFRL-SN-RS-TR-1999-48, Vol. II (of two), May 1999.

8. B. Himed, Y. Salama and J. H. Michels, "Improved Detection of Close Proximity Targets Using Two-Step NHD," *Proc. IEEE International Radar Conference*, Washington D.C, May 7-12, 2000.

9. M. Rangaswamy, B. Himed, and J. H. Michels, "Performance Analysis of the Non-homogeneity Detector," Proc. IEEE National Radar Conference, Atlanta, Georgia, May 2001.

10. M. Soumekh, "Moving Target Detection in Foliage Using Along Track Monopulse Synthetic Aperture Radar Imaging," *IEEE Transactions on Image Processing*, vol. 6, no. 8, pp. 1148-1163, August 1997.

11. M. Soumekh, "Signal Subspace Fusion of Uncalibrated Sensors with Application in SAR and Diagnostic Medicine," *IEEE Transactions on Image Processing*, vol. 8, no. 1, pp. 127-137, January 1999.

12. M. Soumekh, Synthetic Aperture Radar Signal Processing with Matlab Algorithms, New York: Wiley, 1999.

13. M. Soumekh, "Wavefront-Based Synthetic Aperture Radar Signal Processing," *Frequenz*, pp. 99-113, March/April 2001 (special issue on SAR).

14. J. Ender, "Linear and Non-Linear Techniques for Multi-Channel SAR Image Generation," *Proceedings of EUSAR*, May 23-25, 2000.

15. J.W. Goodman, *Statistical Optics*, New York: Wiley, 1985.

16. M. Soumekh and B. Himed, "SAR-MTI Processing of Multi-Channel Airborne Radar Measurement (MCRAM) Data," *Proc. IEEE Radar Conference,* Long Beach, May 2002.

17. J. Curlander and R. McDonough, *Synthetic Aperture Radar*, Wiley, 1991.

18. M. Soumekh, "Bistatic synthetic aperture radar inversion with application in dynamic object imaging," *IEEE Transactions on Signal Processing*, vol. SP-39, no. 9, pp. 2044-2055, September 1991.